République Algérienne Démocratique et Populaire

Kasdi Merbah University, Ouargla
Faculty of Hydrocarbons, Renewable Energy, and Earth and Space Sciences, Ouargla

2eme année LMD Master Petroleum geology

THE TITLE :

Advanced Borehole Imaging for Structural Characterization of the Hassi Messaoud Nord Oil Fiel

production:

- **Dali Hichem**

Supervisor :

* **Pr. Oualid Melouah**

Co-Supervisor: Pr. Medjani Fethi

ANNEE 2024-2025

Deepest

I would like to express my deepest gratitude to my mother, whose unwavering support, guidance, and sacrifices have played a crucial role in my academic journey. Her strength and dedication have been a constant source of motivation

Abstract :

This study focuses on the application of advanced borehole imaging technologies — UBI (Ultrasonic Borehole Imager), UBMI (Ultrasonic Borehole Micro-Imager), CBIL (Circumferential Borehole Imaging Log), and Earth Imager — in the structural characterization of the Hassi Messaoud oil field, one of Algeria's most productive hydrocarbon reservoirs.

Through the integration of these high-resolution tools, we were able to obtain detailed images of borehole walls, allowing for the identification and interpretation of key geological features such as fractures, faults, bedding planes, and breakout orientations. The interpretation of these images provided valuable insights into the in-situ stress regime, fracture networks, and structural heterogeneities that directly influence reservoir behavior and productivity.

The results demonstrate the effectiveness of combining these imaging technologies in improving geological models and optimizing well placement and reservoir management strategies. This study highlights the critical role of borehole imaging in enhancing the understanding of subsurface structures in complex petroleum systems like Hassi Messaoud.

Keywords: UBI . CBIL. UBMI. imaging

Résumé :

Cette étude porte sur l'application de technologies avancées d'imagerie de forage — UBI (Ultrasonic Borehole Imager), UBMI (Ultrasonic Borehole Micro-Imager), CBIL (Circumferential Borehole Imaging Log) et Earth Imager — à la caractérisation structurale du champ pétrolier de Hassi Messaoud, l'un des réservoirs d'hydrocarbures les plus productifs d'Algérie.

L'intégration de ces outils haute résolution nous a permis d'obtenir des images détaillées des parois des forages, permettant l'identification et l'interprétation de caractéristiques géologiques clés telles que les fractures, les failles, les plans de stratification et les orientations des ruptures. L'interprétation de ces images a fourni des informations précieuses sur le régime de contraintes in situ, les réseaux de fractures et les hétérogénéités structurales qui influencent directement le comportement et la productivité du réservoir.

Les résultats démontrent l'efficacité de la combinaison de ces technologies d'imagerie pour améliorer les modèles géologiques et optimiser le placement des puits et les stratégies de gestion des réservoirs. Cette étude souligne le rôle crucial de l'imagerie de forage dans la compréhension des structures souterraines des systèmes pétroliers complexes comme celui de Hassi Messaoud.

Mots-clés : imaging . UBI . CBIL. UBMI

ملخص :

تركز هذه الدراسة على تطبيق تقنيات تصوير الآبار المتقدمة - جهاز تصوير الآبار بالموجات فوق الصوتية (UBI)، وجهاز تصوير الآبار المجهري بالموجات فوق الصوتية (UBMI)، وسجل تصوير الآبار المحيطي (CBIL)، وجهاز تصوير الأرض - في التوصيف الهيكلي لحقل حاسي مسعود النفطي، أحد أكثر مكامن الهيدروكربون إنتاجية في الجزائر.

بفضل دمج هذه الأدوات عالية الدقة، تمكنا من الحصول على صور مفصلة لجدران الآبار، مما سمح بتحديد وتفسير السمات الجيولوجية الرئيسية، مثل الكسور والصدوع ومستويات التراكب واتجاهات الاختراق. وقد وفّر تفسير هذه الصور رؤى قيّمة حول نظام الإجهاد في الموقع، وشبكات الكسور، والتباينات الهيكلية التي تؤثر بشكل مباشر على سلوك وإنتاجية المكمن.

تُظهر النتائج فعالية دمج تقنيات التصوير هذه في تحسين النماذج الجيولوجية وتحسين وضع الآبار واستراتيجيات إدارة المكمن. تسلط هذه الدراسة الضوء على الدور الحاسم الذي تلعبه تقنية تصوير الآبار في تعزيز فهم الهياكل تحت السطحية في أنظمة البترول المعقدة مثل حاسي مسعود.

الكلمات المفتاحية: UBI . UBMI.CBIL . تقنيات التصوير

INTRODUCTION

INTRODUCTION

The Hassi Messaoud oil field, one of Algeria's most significant and productive hydrocarbon reservoirs, serves as a cornerstone of the country's energy sector (Sonatrach, 2019; Oukaci et al., 2012). The field's immense economic value underscores the importance of a thorough understanding of its geological structure, which is crucial for optimizing extraction techniques, enhancing reservoir management, and ensuring sustained productivity (Bencheikh-Lehocine et al., 2005; Bekkouche et al., 2017).

Given the reservoir's complex subsurface characteristics, precise geological characterization plays a critical role in maximizing recovery rates and informing long-term field development strategies (Guiraud et al., 2000; DGH Algeria, 2021).

In recent years, advancements in borehole imaging technologies have provided unprecedented opportunities for in-depth structural analysis of subsurface formations. Among these, the Ultrasonic Borehole Imager (UBI), Ultrasonic Borehole Micro Imager (UBMI), and Circumferential Borehole Imaging Log (CBIL) have emerged as powerful tools for obtaining high-resolution visualizations of the borehole wall (Schlumberger, 2014; Rider & Kennedy, 2011). These advanced imaging methods offer vital insights into the internal structure of the reservoir, facilitating the detection and analysis of key geological features, including fractures, bedding planes, and fault systems (Zemskova et al., 2019; Serra, 2007).

These structural elements are essential to understanding fluid flow dynamics, reservoir connectivity, and overall production potential (Nelson, 2001; Aguilera, 1995).

This study aims to assess the application and efficacy of UBI, UBMI, and CBIL in the structural characterization of the Hassi Messaoud reservoir. By integrating borehole image data into geological modeling, this research seeks to provide a more refined interpretation of subsurface structures, which can significantly improve reservoir performance (Belhadi et al., 2018; Wu et al., 2020). The ability to identify fractures and faults with high precision enables better prediction of reservoir behavior, enhancing the ability to target optimal zones for hydrocarbon extraction (Lorenz et al., 2002).

Furthermore, detailed imaging allows for more accurate assessment of the reservoir's heterogeneity, which is crucial for developing tailored strategies to optimize fluid recovery (Laubach et al., 2019; Békri et al., 2014).

The study will analyze borehole image data to assess the effectiveness of these imaging technologies in mapping and understanding the structural intricacies of the reservoir. By applying these tools in combination with traditional geological analysis, the research aims to contribute to a more accurate and comprehensive geological understanding of the Hassi Messaoud oil field (Tari et al., 2012). This, in turn, will support enhanced hydrocarbon recovery techniques and facilitate informed decision-making in field development, ultimately contributing to the long-term sustainability and profitability of Algeria's oil and gas sector (IEA, 2022).

Through this investigation, the study also seeks to advance the application of modern imaging technologies in reservoir management, paving the way for more efficient and economically viable extraction practices (Mendoza et al., 2015; Halliburton, 2020).

Keywords

Hassi Messaoud oil field, borehole imaging, UBI, UBMI, CBIL, fracture characterization, structural analysis, reservoir heterogeneity, geological modeling, subsurface structures, hydrocarbon recovery, reservoir management, fault systems, fluid flow dynamics, high-resolution logging, acoustic imaging, resistivity imaging, advanced logging tools.

CHAPITER 1 :

General Overview of the Hassi Messaoud Field

Part 1: General Overview

1. Geographical Location of the Hassi Messaoud Field:

The Hassi Messaoud field is located in the **northeastern part of the Algerian Sahara**, approximately **850 km southeast of Algiers** and **350 km from the Algerian-Tunisian border**.
The field spans an area of **2500 km²**, with an oil-impregnated surface of about **1600 km²**.

It is bounded:

- **To the north** by **Touggourt**
- **To the south** by **Gassi Touil**
- **To the west** by **Ouargla**
- **To the east** by **El Bourma**

Its location in **Lambert coordinates** is as follows:

- **X = 790,000 – 840,000 East**
- **Y = 110,000 – 150,000 North**

It lies between latitudes **31°30' and 32°00'**, and longitudes **5°40' and 6°20'**.

(Documents « SONATRACH 2004» : Géologie de Hassi-Messaoud).

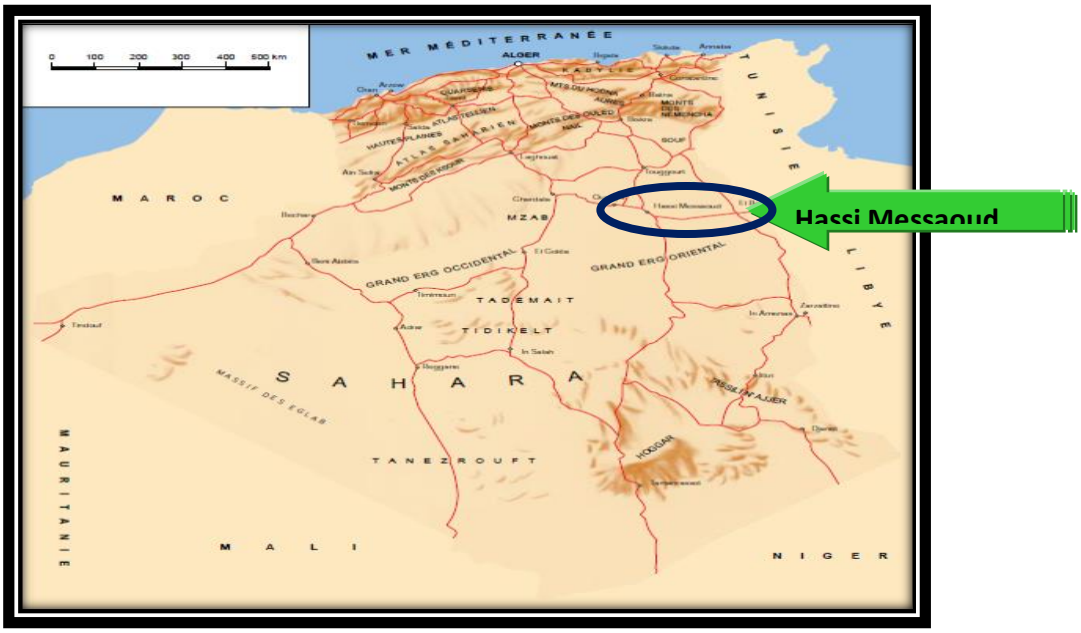

Figure 2: Geographical Location of the Hassi Messaoud Field

(Source: Schlumberger–Sonatrach WEC 2007).

2. Presentation of the Hassi Messaoud Field:

The Hassi Messaoud field is located in the Oued Mya Basin in the northern Sahara, about 950 km southeast of Algiers and 350 km from the Tunisian border. It covers an area of **1600 km²**.

This field is characterized by a **Cambro-Ordovician formation** with the following features:

- A depth ranging from **3000 m to 3500 m**
- An approximate thickness of **200 m**
- **Light crude oil** with an API gravity of **45.04**
- An initial reservoir pressure of **482 kgf/cm²**, with a **bubble point** between **140 and 200 kgf/cm²**

The oil reservoir is composed of four main layers (in increasing depth):
Ri, Ra, R2, and R3
(Source: SONATRACH 2004 – Geology of Hassi Messaoud).

2.1 Exploration History:

The Hassi Messaoud oil field, located in the Berkine Basin, is one of the largest oil fields in Algeria. Its exploration history represents a key milestone in the development of the national oil industry.

Geological interest in the region dates back to the early 1950s, when the French Petroleum Company (CFP), through its subsidiary REPA (Autonomous Authority for Algerian Petroleum), launched a series of geophysical surveys, notably magnetic and gravimetric surveys. These campaigns revealed a strong magnetic anomaly in the southeastern Algerian Sahara, suggesting the presence of a deep anticlinal structure.

In June 1956, drilling of the MD-1 well was initiated based on this geophysical data. Although it was not immediately productive, it helped identify reservoir formations within the fractured Cambrian basement.

It was in November 1957 that the OMG-1 well (Oued Mya Field) confirmed the presence of commercially viable oil, marking the true beginning of the Hassi Messaoud oil field. The main reservoir consists of sandstones at the base of the Cambrian, resting on the Precambrian basement and saturated with hydrocarbons.

This success led to an intensive drilling campaign, which confirmed the field's extension. It was later found to cover more than 1,500 km². This development marked the start of a new energy era for Algeria, laying the foundations for its oil sovereignty after independence. *(Documents « SONATRACH 2004» : Géologie de Hassi-Messaoud).*

3. Regional Geology of the Algerian Sahara:

The geological history of Algerian sedimentary basins is part of the global geodynamic process of plate tectonics, which has divided Algeria into two main domains:

- **To the north**: the Alpine Algeria
- **To the south**: the Saharan Platform

➢ Geological Context of the Saharan Platform:

The Saharan Platform is a vast and geologically stable region that has been shaped since the Paleozoic era. It includes a number of sedimentary basins distributed across three major provinces:

➢ The Western Province:

This province includes the following basins:

- Béchar
- Tindouf
- Reggane
- Ahnet
- Mouydir
- Timimoun
- Sbaa

➢ The Triassic Province:

This province is characterized by several structural features, including:

- The Tilhemt Arch and the Talemzane High
- The Djemaa-Touggourt Structural System
- The Dahar Môle

- The El Biod High

➢ **The Eastern Province:**

This province is composed of the following basins:

- **Illizi**
- **Ghadames**

These two basins are separated by the **Ahara Môle**.

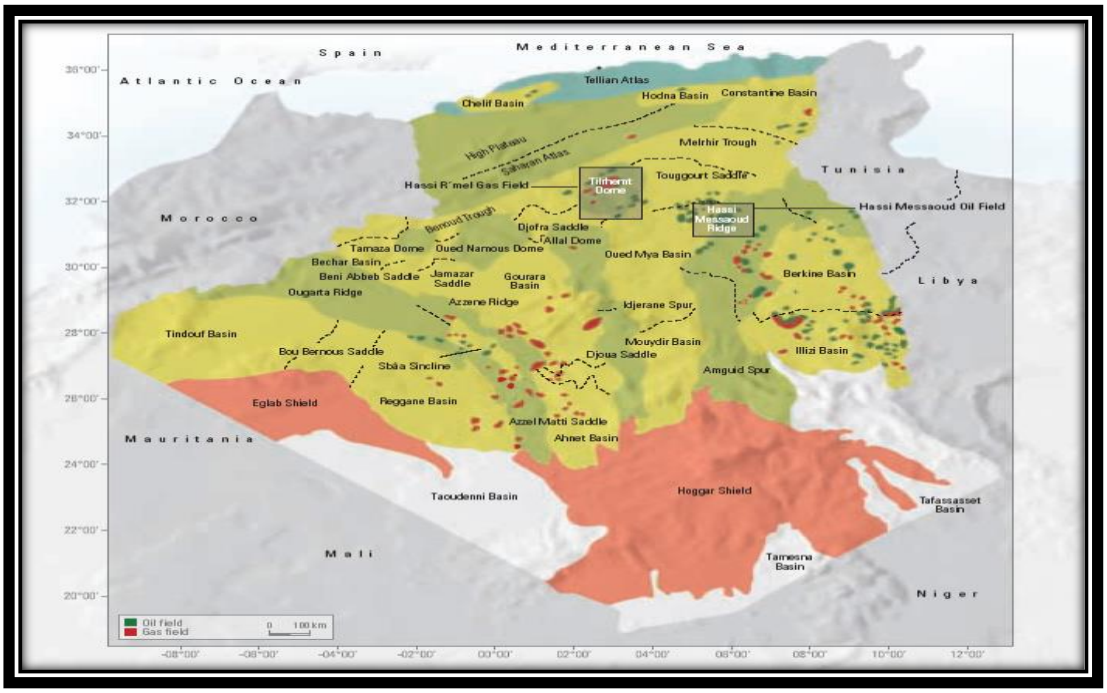

(Source: Schlumberger – Sonatrach WEC 2007 document)

.

Figure1: **Distribution of Algerian Sedimentary Basins**
(Document Schlumberger-Sonatrach WEC 2007).

Part 2: Local Geological Framework

1. Local Geology of the Hassi Messaoud Field:

The Hassi Messaoud field is located in the central part of the **Triassic Province**. In terms of surface area and reserves, it is the **largest oil field in Algeria**, covering nearly **2200 km²**.

It is bordered by:

- **Northwest**: the **Ouargla fields** (Gellala, Ben Kahla, and Haoud Berkaoui)

- **Southwest**: the **El Gassi, Zotti, and El Agreb fields**
- **Southeast**: the **Rhourde El Baguel and Mesdar fields**

Geologically, the field is bounded by:

- **West**: the **Oued M'ya depression**
- **South**: the **Amguid El Biod Môle**
- **North**: the **Djamaa-Touggourt structure**
- **East**: the **Dahar high, Rhourde El Baguel, and the Ghadames depression**

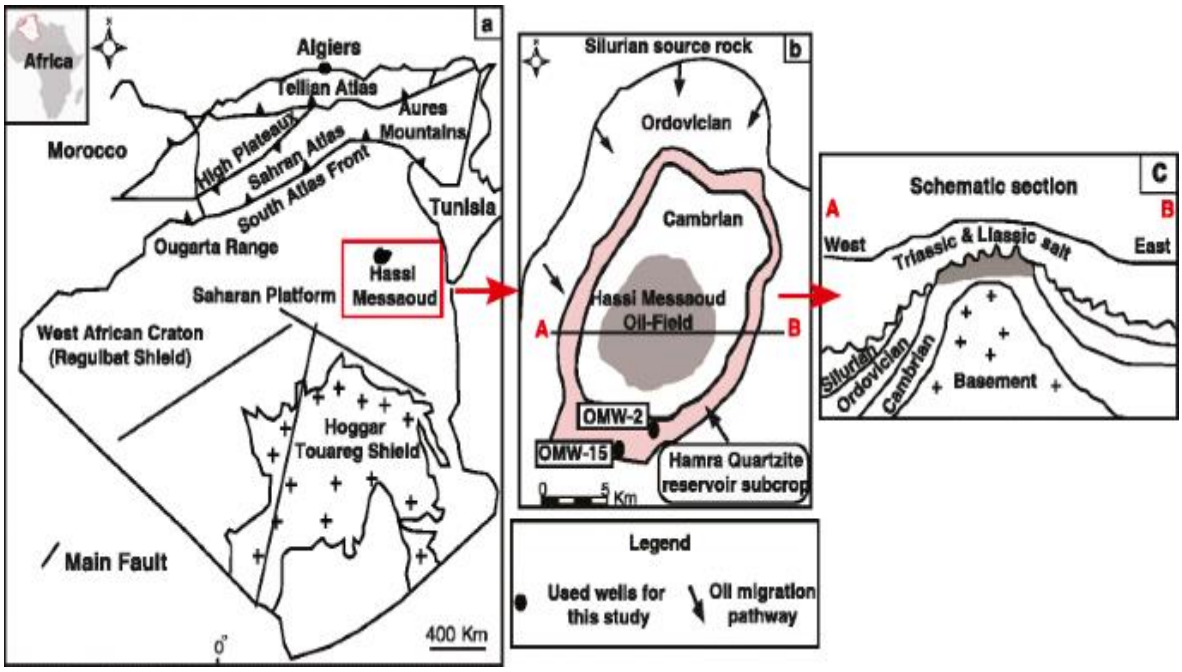

Figure 3: Geological Setting of the Hassi Messaoud Field

(Benayad et al.,2013, Arabian Journal of Geosciences .).

1.2. Hydrogeology of the Hassi Messaoud Field:

The underground resources of the region are not limited to hydrocarbons extracted in the Algerian Sahara, particularly in Hassi Messaoud, Hassi R'mel, and Hassi Berkine. This region is also rich in **strategic groundwater resources**.
The aquifers of Hassi Messaoud are part of the **North Western Sahara Aquifer System (NWSAS)**, a large transboundary system shared by **Algeria, Libya, and Tunisia**, containing significant water reserves.
This system extends over an area of more than **1 million km²**, with approximately **70% located in Algeria**, **8% in Tunisia**, and **20% in Libya**.

In the Algerian Sahara, **Meso-Cenozoic detrital and carbonate formations** form the aquifers used to meet various **domestic, agricultural, and industrial** water needs.

Hassi Messaoud region contains **two main aquifers**:

- **The Terminal Complex Aquifer (T.C.):**
  This includes the aquifers of the **Mio-Pliocene**, **Eocene**, and **Senonian carbonate** formations.
- **The Continental Intercalaire Aquifer (C.I.):**
  This is a **multi-layer aquifer** consisting of formations from the **Albian**, **Barremian**, and **Neocomian** periods.

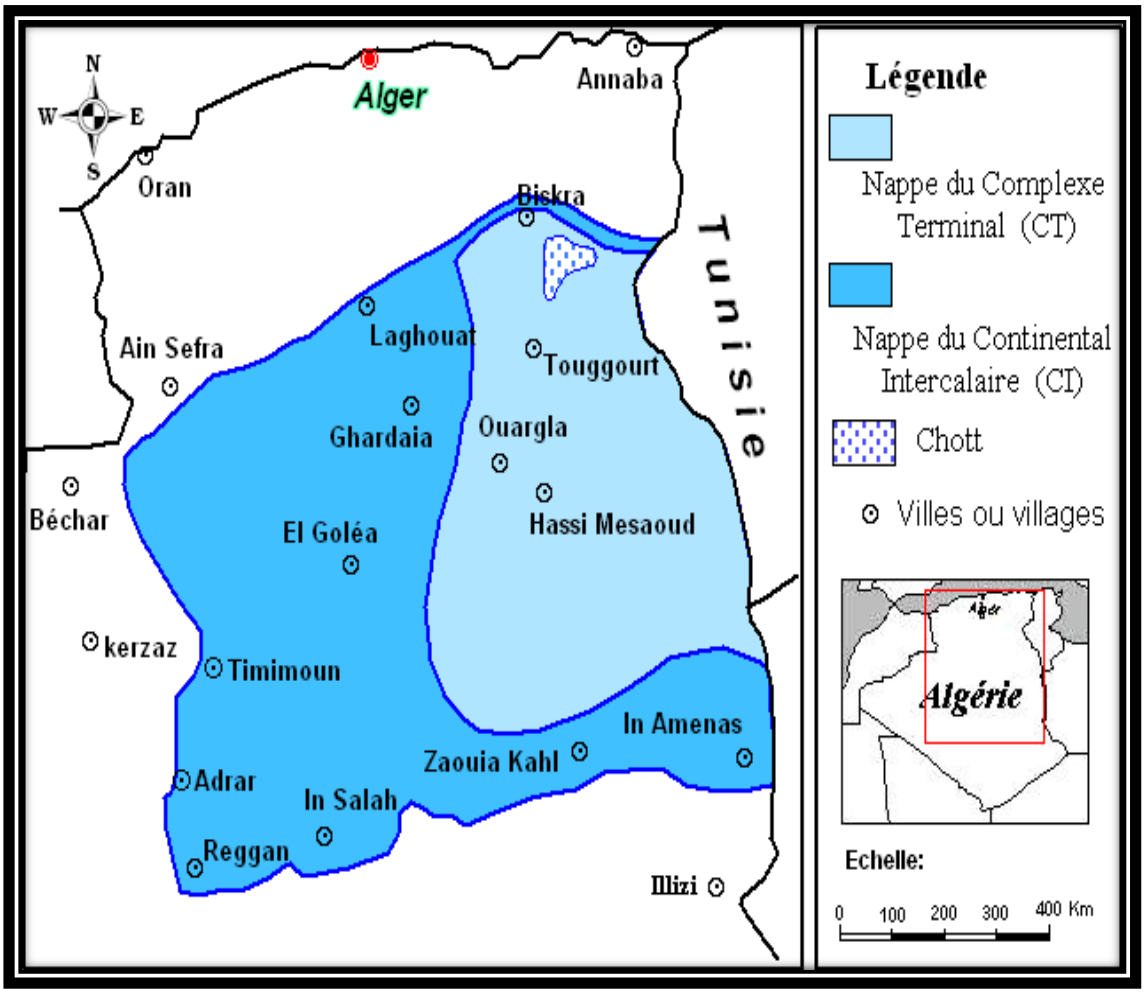

Figure 4: Aquifers of the North Western Sahara

(Excerpt from the 2002 Communications Proceedings).

1.3. Lithostratigraphy of the Hassi Messaoud Field:

1.3.1. Cenozoic:

1.3.1.1. Mio-Pliocene (thickness ≈ 240 m):

Composed of:

- White sand with thin layers of soft to pasty reddish-brown clay,
- White, chalky, soft limestone with varicolored clay beds,
- Gray-brown marl, highly sandy.

These continental sandy deposits were laid down via channels (showing great horizontal and vertical grain size variability). They are unconsolidated and highly porous, leading to partial or total fluid losses and collapse risks during drilling. They rest on the Eocene with an erosional contact.

1.3.1.2. Eocene (thickness ≈ 120 m):

Composed of:

- Reddish-brown, highly sandy clay,
- Marl with thin beds of white anhydrite,
- Chalky dolomitic limestone, sometimes with flint nodules.

The Tertiary holds a potable water aquifer complex.

1.3.2. Mesozoic:

1.3.2.1. Cretaceous:

a. Senonian: Composed of two levels:

- **Carbonate unit** (thickness ≈ 107 m): dolomitic limestone with thin anhydrite beds.
- **Lagoonal unit:** Two sub-units with lagoonal facies:
    - **Anhydritic unit** (thickness ≈ 219 m): white crystalline anhydrite, medium-hard dolomite, marl, and argillaceous-dolomitic limestone.
    - **Saliferous unit** (thickness ≈ 140 m): massive salt with traces of anhydrite.

b. Turonian (thickness ≈ 70–120 m): Carbonate formations composed of limestone, chalk, dolomite, and some clay layers.

c. Cenomanian (thickness ≈ 145 m): Alternating anhydrite and red clay, gray marl, and dolomite.

d. Albian (thickness ≈ 350 m): Fine sandstones and sands interbedded with silty clays.

e. Aptian (thickness ≈ 25 m): Two crystalline dolomite beds enclosing a clay level.

f. Barremian (thickness ≈ 280 m): Fine carbonated sandstones alternating with clay layers and dolomitic sandstones.

g. Neocomian (thickness ≈ 180 m): Microcrystalline dolomite, marls, and clays with thin sandstone beds.

1.3.2.2. Jurassic:

a. Upper Jurassic (Malm) (thickness ≈ 225 m): Clay and marl deposits with interbedded limestone and dolomite, with occasional traces of anhydrite.

b. Middle Jurassic (Dogger): Two levels:

- **Argillaceous** (thickness ≈ 105 m): Silty clays, dolomitic marls with thin sandstone beds.
- **Lagoonal** (thickness ≈ 210 m): Anhydrite, argillaceous dolomite, marl.

c. Lower Jurassic (Lias) (thickness ≈ 300 m): Divided into five levels:

- **LD1**: Gray, hard dolomite, white anhydrite with occasional silty clay beds (≈ 65 m),
- **LS1**: Salt and clay beds with white anhydrite (≈ 90 m),
- **LD2**: Massive microcrystalline dolomites with marly interbeds containing chlorinated calcium-rich waters (≈ 55 m),
- **LS2**: Massive translucent white salt with argillaceous-saline interbeds (≈ 60 m),
- **LD3**: Marls with dolomitic beds (≈ 30 m).

1.3.2.3. Triassic:

Four levels represented:

a. Saliferous, divided into three sub-horizons:

- **TS1**: Massive salt with anhydrite beds and dolomitic clay interbeds (≈ 46 m),
- **TS2**: Massive salt with white anhydrite and silty gypsiferous clays (≈ 189 m),
- **TS3**: Massive salt with traces of soft silty clays (≈ 202 m).

TS2 and TS3 are known for flowing clays.

b. Argillaceous: More or less silty, dolomitic, and anhydritic clays with salt beds at the top (≈ 113 m).

c. Sandy: Fine sandstones with clay cement (≈ 35 m).

d. Volcanic: Altered andesites alternating with clays (0–92 m), overlying Paleozoic formations with an angular unconformity (Hercynian).

The clay-sandstone Triassic (TAG) is prone to variable fluid losses across the field. It unconformably overlies the Cambrian at the field's center and the Ordovician on its flanks.

1.3.3. Paleozoic:

1.3.3.1. Ordovician

In its complete representation, it includes four units:

- **Hamra Quartzites** (12–75 m): Locally coarse quartzites with occasional clay interbeds.
- **El Atchane Sandstones** (25 m): Fine, clay-cemented, bituminous sandstones.
- **El Gassi Clays** (50 m): Schistose, carbonate-rich green and black clays.
- **Alternating Zone** (20 m): Hardened clays alternating with equidimensional quartzite beds and medium to fine sandstones.

1.3.3.2. Cambrian

Mainly heterogeneous sandstones, ranging from fine to very coarse, interbedded with argillaceous-micaceous siltstones, known as the "Grès de Messaoud." Three lithozones can be distinguished: **R1 (Ri + Ra), R2, and R3**.

1.3.3.3. Infra-Cambrian

The oldest geological unit identified in the northern part of the structure by well Omg47 at a depth of 4092 m. It is composed of red argillaceous sandstones (≈ 45 m).

1.3.4. Basement

Encountered at around **4000 m depth**, it consists of **pink porphyroid granite with two micas**.

(Source: SONATRACH 2004 – Geology of Hassi Messaoud).

ERE	SYST	ETAGES		Ep moy	DESCRIPTION
CENO-ZOIQUE	NEOGENE	MIO-PLIOCENE discordance alpine		240	Sable, calcaire, marne sableuse
		EOCENE		120	Sable, calcaire à silex
MESOZOIQUE	CRETACE	SENONIEN	CARBONATE	107	Calcaire, dolomie, anhydrite
			ANHYDRITIQUE	219	Anhydrite, marne, dolomie
			SALIFERE	140	Sel massif et traces d'anhydrite
		TURONIEN		90	Calcaire crayeux avec quelques niveaux argileux
		CENOMANIEN		145	Anhydrite, marne, dolomie
		ALBIEN		350	Grés, sable avec intercalations d'argile silteuse
		APTIEN		25	Dolomie cristalline avec niveau argileux, calcaire
		BARREMIEN		280	Argile, grés, dolomie
		NEOCOMIEN		180	Argile, marne, dolomie, grés
	JURASSIQUE	MALM		225	Argile, marne, calcaire, grés et traces d'anhydrite
		DOGGER	ARGILEUX	105	Argile silteuse, marne dolomitique avec fines passées de grés
			LAGUNAIRE	210	Anhydrite, marne dolomitique, marne grise
		LIAS	L.D 1	65	Dolomie, anhydrite, argile
			L.S 1	90	Alternances sel, anhydrite et argile
			L.D 2	55	Anhydrite et dolomie cristalline
			L.S 2	60	Alternances sel et argile
			L.D 3	30	Alternances de dolomie et de marne
	TRIAS	SALIFERE	TS 1	46	Alternances de sel, d'anhydrite et de dolomie
			TS 2	189	Sel massif à intercalations d'anhydrite et argile gypsifère
			TS 3	202	Sel massif et traces d'argile
		ARGILEUX		113	Argile rouge dolomitique ou silteuse injectée de sel et d'anhydrite
		GRESEUX		35	Grés, argile
		ERUPTIF discordance hercynienne		0-92	Andésites altérées
PALEOZOIQUE	ORDOVICIEN	QUARTZITES D'EL HAMRA		75	Quartzites fines avec traces de tigillites
		GRES D'EL ATCHANE		25	Grés fins à ciment argileux, bitumineux
		ARGILES D'EL GASSI		50	Argiles schisteuses, vertes ou noires, glauconieuses à graptolithes
		ZONE DES ALTERNANCES		20	Alternance de grés et argile. Présence de tigillites
	CAMBRIEN	Ri		50	Grés isométriques, fins, silteux
		Ra		120	Grés à grés quartzitiques anisométriques à niveaux de silts
		R2		100	Grés moyens à grossiers à ciment argileux illitique
		R3		300	Grés grossier à ciment argileux, argile silteuse
	INFRA-CAMBRIEN			45	Grés argileux rouges
SOCLE					Granite porphyroïde rose

Figure 05: Lithostratigraphic Column of the Hassi Messaoud Field
(Source: "SONATRACH" – Geology of Hassi Messaoud, 2004).

2. Petroleum System :

2.1. Source Rock:

- **Silurian:**
  The Silurian shales constitute the source rock generating hydrocarbons across the entire Saharan platform. This source is represented by black, calcareous, radioactive shales, very rich in organic matter, with a thickness ranging from 20 to 70 meters.
  The organic matter is amorphous in nature. The presence of Tasmanites confirms the marine origin of this matter and its evident petroleum potential. Currently, it is believed that after the primary expulsion of hydrocarbons generated during the Paleozoic, a second, more significant phase of generation occurred, which ceased at the end of the Cretaceous due to a decrease in subsidence.
  The Silurian is preserved in the north of the Hassi Messaoud field, to the west (in the Oued Mya Basin), to the southwest (Mouydir Basin), and to the east (Berkine Basin).

2.2. Cap Rocks:

The Ordovician reservoirs are sealed by volcanic outflows and by thick evaporite sequences of Triassic or Jurassic age.

2.3. Traps:

Traps are the most favorable zones for hydrocarbon accumulations, characterized by lower pressure and temperature than those of the source rocks, and by a barrier that forces hydrocarbons to accumulate. (A. PERRODON, 1985).
There are three types of traps:

- **Structural Traps:** Formed as a result of tectonic movements such as anticlines or fault traps.
- **Stratigraphic Traps:** Created by the transition between permeable and impermeable environments, such as sandstone lenses or pinch-outs.
- **Mixed Traps:** These are both structural and stratigraphic, such as the HMD structure (an anticline truncated by the Hercynian unconformity).

In the Oued Mya Basin and the northeast of Hassi Messaoud, the known traps are mixed, combining both structural and stratigraphic characteristics.

2.4. Hydrocarbon Migration:

The hydrocarbon accumulations in the Hassi Messaoud field and nearby fields likely originate from the Ghadames and Illizi Basins to the east and the Oued Mya Basin to

the west.
Primary migration and charging occurred within the Silurian, followed by secondary migration through Triassic sandstone layers along the Hercynian unconformity.
The Cambro-Ordovician reservoirs, outcropping at the Hercynian unconformity, are charged via the Triassic sandstones and the erosional surface located updip to the north and northwest along the migration path.

2.5. Reservoir Description of the Hassi Messaoud Field:

The main reservoir of the Hassi Messaoud field is heterogeneous, discontinuous, and anisotropic. This anisotropy is mainly due to the presence of silts. Depending on their extent, these impermeable silt beds can act as barriers to fluid segregation. Their extent, thickness, location, and density within the Cambrian Ra series are key elements of the correlation presented.
(*S. Mekmouche, "Description of the Hassi Messaoud Reservoir", Forum Stimulation SH/DOWELL, Hassi Messaoud, 1994.*)

Four (4) lithozones can be distinguished:

- **Lithozone R3:** Average thickness: 370 m
  Composed of feldspathic and micaceous sandstones with medium to very coarse grains, conglomeratic at the base, with abundant clay cement. Also includes ferruginous sandstone beds and silty clays.
- **Lithozone R2:** Average thickness: 100 m
  Composed of micaceous, medium to coarse sandstones, poorly sorted, with fairly abundant clay cement and interbedded silts. Cross-bedding is common.
- **Lithozone Ra:** Average thickness: 125 m
  Composed of anisometric, medium to coarse quartzitic sandstones with clayey and siliceous cement. Includes numerous centimeter- to decimeter-thick siltstone layers. Cross and horizontal bedding are observed, and tigillites are present in the upper part. The central part of the Ra series has been eroded.
- **Lithozone Ri:** Average thickness: 42 m
  Composed of fine, well-sorted, isometric quartzitic sandstones, glauconitic, with clayey and siliceous cement, and abundant tigillites.

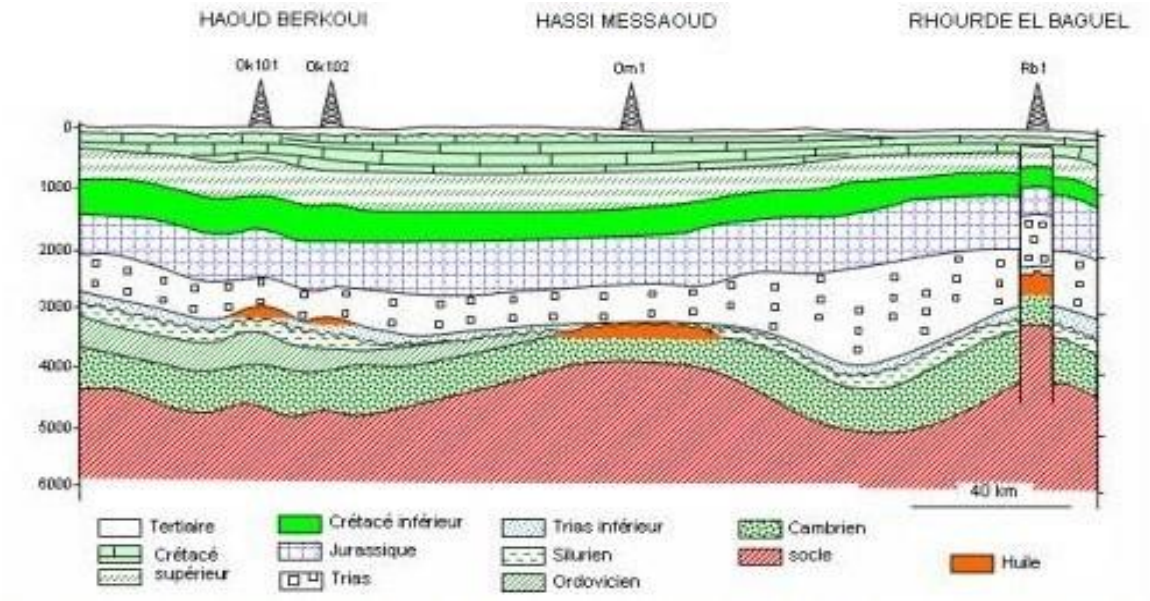

Figure 06: Geological cross-section of the main reservoir of the Hassi-Messaoud field.

(Designed by Hassi Messaoud, published by C. Sallé and J. Debyser, Technip 1976)..

2.6. Zoning of the Hassi Messaoud Field:

Currently, the field is divided into **25 production zones**, based on **reservoir pressure**. These zones are relatively independent and consist of sets of wells communicating with each other.

Some zones have boundaries that align well with the structural features of the field, while others have boundaries that are less clearly defined from a geological perspective.

The Hassi Messaoud field is divided into **two distinct parts**:

- **Northern Field**: includes wells such as **OMM13, OMN25, OMO14, OMP17, OMJ11, OMK20, OML65, ONI45, ONM43**
- **Southern Field**: includes the **MD** wells, numbered chronologically For example: **MD1, MD2, MD3, MD4**, etc.

The well naming system combines **geographical identification** with **chronological numbering**

Example – OMN25:

- **O**: Ouargla permit - **M**: 1600 km² grid square - **N**: 100 km² sub-square **2**: X-axis coordinate - **5**: Y-axis coordinate

(Documents « SONATRACH 2004» : Géologie de Hassi-Messaoud).

3. Tectonic and Structural Framework :

3.1. Tectonics of the Hassi-Messaoud Field:

It is characterized by compressive forces leading to brittle tectonics, represented by major vertical faults. These are offset by a network of faults trending NE-SW with dextral (right-lateral) movement, and NW-SE with sinistral (left-lateral) movement. This fault system was interpreted by **Ball (1980)** as resulting from the collision of two rigid continental blocks: the **West African Craton** and the **East Saharan High**.

These movements are responsible for the main structural axes of the Saharan platform and for its division into sedimentary basins (**Sonatrach, 1975**).

The structure of the Hassi Messaoud field appears as a vast flattened **anticlinal dome**, with a general **NE-SW orientation**. The faults affecting the reservoir fall into two categories:

- **Faults trending approximately NNE–SSW**, along with other faults **perpendicular to them (NW–SE direction)**. This highlights the **Horst and Graben** tectonic pattern.
- **Fractures without noticeable displacement**, which nonetheless have had a significant impact on reservoir fracturing.
  (*Structure and fracturing of the Hassi Messaoud field, M. Ruhland, J. Thouvenin, 1971*)

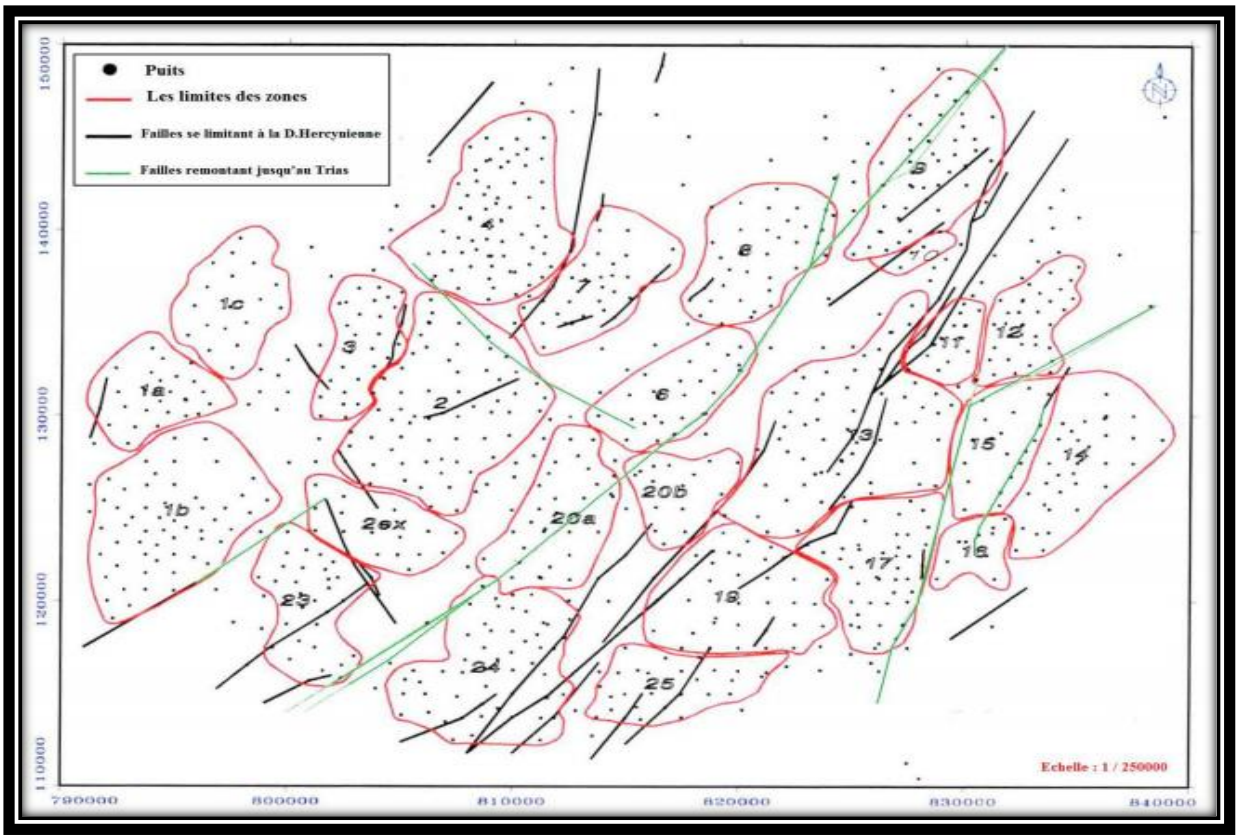

Figure 07 : Structural map and zoning of the Hassi Messaoud field.
(Source: Sonatrach / Production Division – Internal Report, 2002)

3.2. Structural Evolution of the Hassi Messaoud Field:

The structural evolution of the field is the result of several tectonic phases that can be summarized chronologically as follows:

3.2.1. Pre-Triassic Structuring

• Pan-African Phase:
This compressional phase, oriented E-W, is attributed to a continental collision between the rigid West African craton and the more ductile East African block. It caused brittle tectonics, represented by a network of faults oriented NE-SW and NW-SE, followed by intense erosion lasting until the Cambrian, leading to the formation of a planation surface known as the **infra-Tassilian surface**. This pediplain marks the beginning of the cratonic history of the Sahara. *(Bertrand & R. Caby, 1978)*

Extensional movements oriented NW-SE occurred during the Cambro-Ordovician, leading to the stretching of the continental crust, followed by tectonic subsidence and later thermal subsidence. This extension triggered reactivation of pre-existing basement faults (NE-SW orientation), accompanied by volcanic activity.
(Beicip/Franlab, 1979)

• Early Eo-Caledonian or Pre-Tremadocian Phase:
Dated to approximately 500 million years ago, this phase is marked by the transgression of isometric sandstones (Ri), known from the flanks of the field, following the deposition of the Ra reservoir.
A **Tardi-Cambrian** structure developed, accompanied by erosion and faulting along NE-SW orientations, also associated with volcanic activity. *(Beicip/Franlab, 1979)*

• Caledonian Phase:
Dated around 400 million years ago, this phase is regionally evidenced by the absence of Devonian and Carboniferous sediments across the El Biod high.
It is important to note that non-deposition of these sediments is preferred over the hypothesis of Hercynian erosion, since reworked facies at the base of the Triassic sandstones originate from the Cambro-Ordovician. This phase is believed to have started in the Silurian or Early Devonian. *(MASSA-NICOL, 1971)*

• Hercynian Phase:
Dated between 225 and 280 million years ago, this phase is responsible for a significant doming structure oriented NE-SW, accompanied by fault activity in the same direction, which segmented the reservoir into blocks with individual behaviors (Horst and Graben structures).
There is evidence of erosion of the entire Paleozoic cover directly above the field, as seen by the radial pattern of large incised valleys.
During this phase, compressive stress is oriented NW-SE, i.e., **perpendicular to the major structural features**.

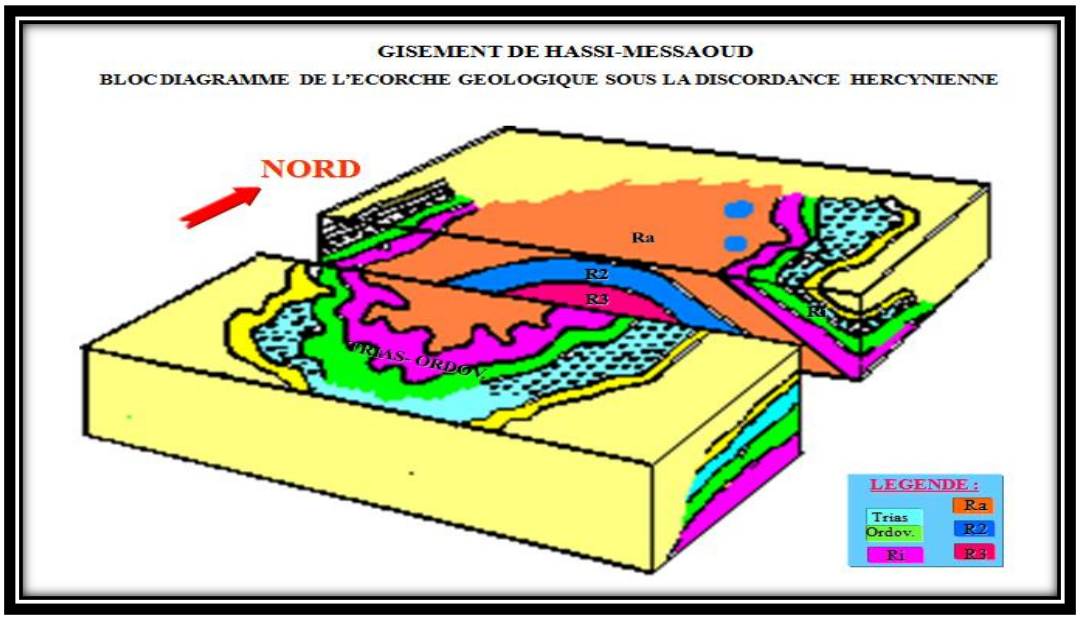

Figure. 08: The Hercynian Unconformity**.**

(Source: "SONATRACH" – Geology of Hassi Messaoud, 2004).

3.2.2. Post-Triassic Structuring:

The effects of this phase are relatively minor, corresponding to only **50 to 100 meters of structural closure** (2950–3050 m). These deformations are accompanied by a **tilting toward the NW** of approximately 200 meters between the SE and NW parts of the field, which occurred during the **Mesozoic**.
The **N–S closure** is much greater than the **W–E closure** and could be attributed to **Eocene-aged movements**, part of the **Atlas tectonic phase**, with a **NNW–SSE compression direction** (Beicip/Franlab, 1979).

- **Austrian Phase:**
  Dated to approximately **100 million years ago**, this phase was marked by **E–W shortening**, which increased the structural closure and caused fracturing along pre-existing faults, likely reactivating them.
  It is nearly **synchronous with hydrocarbon emplacement**, as generation began in the **Jurassic** and continued through the **Cretaceous**.
- **Atlas Phase:**
  This phase involved **NNE–SSW compression**, occurring **after hydrocarbon formation**. It is thus **likely responsible for the creation of permeability barriers** due to the offset of reservoir layers.

3.2.3. Present-Day Structuring:

This structuring displays a **300-meter closure** between the flanks and the top of the reservoir. It is **compressive**, with **N–S shortening**, and has undergone a **slight epeirogenic adjustment**.
The current structure has a general **NE–SW elongation**, showing **local culminations** with amplitudes on the order of **hundreds of meters**.
The **known fault displacements** do **not exceed 70 to 80 meters**. (Beicip/Franlab, 1979)

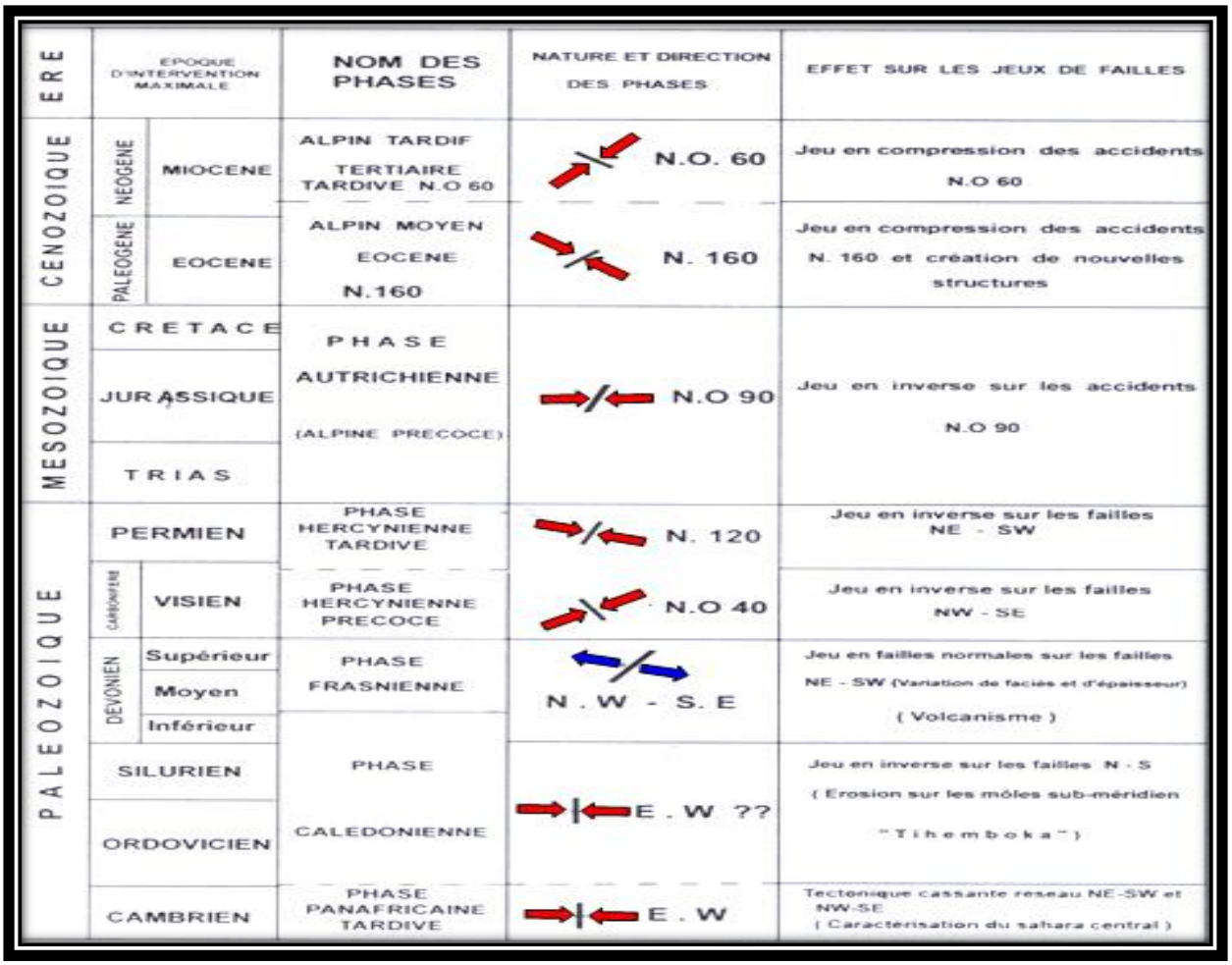

Figure 09: Major tectonic phases identified within the Saharan platform**.**
(After Boudjema (1987) and Beicip (1975). Modified by K. BOUSLAH)

4. "Fracture Analysis and Structural Characterization of Cambrian Sandstone Reservoirs Based on Core Data: Methodological Study Applied to Hassi Messaoud North (Gautier et al., 1973)" :

The **Hassi Messaoud oil field**, located in southeastern Algeria approximately 80 km south of the city of Ouargla, is one of the largest and most productive hydrocarbon reservoirs in North Africa. It is situated within the **Saharan Platform**, a geologically stable area hosting deep sedimentary basins. The reservoir rocks primarily consist of **Devonian and Silurian sandstones**, which exhibit various levels of **tectonic fracturing**, greatly influencing fluid flow and reservoir performance.

This study aims to investigate the **fracture networks and tectonic features** within the reservoir using **core sample analysis** and advanced observation techniques. Understanding the structural framework is essential for predicting reservoir behavior, optimizing hydrocarbon recovery, and supporting long-term field development.

A total of **approximately 80 wells** were studied across the Hassi Messaoud field, covering **about 8,200 meters of core material**, and yielding **around 140,000 individual measurements** [Source: Gautier et al.]. Among the analyzed wells, **Well No. 5** was extensively studied using the **developed core method** to map fractures and bedding planes with high accuracy. Other wells were analyzed using simplified logging methods due to the fragmented condition of some older cores.

The methodology applied in this study includes:

- **Core development drawing (carotte développée)**, which involves wrapping core fragments with tracing film (Kodatrace) and mapping all observable geological structures.
- **Rotational core photography** and **fluorescent ink application** for fracture detection.
- **Autoradiography** (Lévêque, 1969) to highlight microfractures using radioactive markers.
- **Measurement of fracture dip and azimuth** using sinusoidal curve interpretation from the developed cores [Source: Gautier et al.; Ruhland, 1969a, 1973].

The observed tectonic elements include:

- Fractures (open and sealed), their dip, orientation, and intersection angles.
- Bedding-plane slip striations.
- Polished fault mirrors and tectonic breccias.
- Stylolites and clay-silt laminae (often referred to as “silts”).

This study not only improves our geological understanding of the Hassi Messaoud reservoir but also enhances the interpretation of **dipmeter logs** and supports more accurate structural modeling. The collected data enables better **correlation with borehole image logs**, ultimately leading to improved reservoir management and more efficient hydrocarbon extraction strategies.

4. Fracturing and Tectonic Analysis on Core Samples: A Methodological Study Applied to the Hassi-Messaoud North Oil Field

Source: Gautier, J.-M., Gruneisen, P., Massa, D., & Ruhland, M. (1973). *Sciences Géologiques*, Bulletin 26(2–3), 115–159. DOI: 10.3406/sgeol.1973.1429

4.1. Introduction :

The Hassi-Messaoud oil field, located in southeastern Algeria, is a major hydrocarbon reservoir composed primarily of fractured Cambrian sandstones. Since its discovery in 1956, the field has been the subject of extensive subsurface studies. However, the role of natural fracturing in influencing fluid flow whether as conduits or barriers has remained complex and insufficiently understood.

In this context, the study by Gautier et al. (1973) aimed to adapt field-based structural geology methods to the analysis of **drilling cores** in order to better understand the **fracture systems and tectonic framework** of the Hassi-Messaoud North sector. The research relied on direct analysis of core samples from over **100 wells** (representing **8,212 meters of core**), using both high-resolution dipmeter logging and developed-core techniques.

4.2. Objectives of the Study

- To identify and characterize tectonic indicators (fractures, striations, breccias) directly on core samples.
- To adapt and test observational and analytical techniques (e.g., developed cores, autoradiography, fluorescent ink) for detecting and orienting fractures.
- To define the fracture network and its spatial relationship with known fault systems through a combination of structural, sedimentological, and logging data.

4.3. Methodology Summary :

- **Study Area**: Hassi-Messaoud North concession (35 km E-W x 25 km N-S).
- **Core Dataset**: 102 wells; 8,212 meters of core; ~140,000 individual structural measurements.
- **Well Example**: *Well No. 5 (Oto 51)* was analyzed in detail using developed-core methods.
- **Techniques Used**:
  - Rotational core photography.
  - Developed-core drawings (wrapping core with Kodatrace sheets).
  - Autoradiography for microfracture detection (Lévêque, 1969).
  - Fluorescent ink application.
  - High-resolution dipmeter (HdT) and magnetic orientation methods.

4.4. Main Results :

A. Fracture Geometry and Frequency

- Most fractures are **subvertical**, with dips >80°, dominating the structural network.

- **Fracture frequency** varied widely between wells but was especially high near major faults.
- **Example**: In *Well Oto 51*, five closely spaced subparallel fractures (N 327/75, 330/80, 352/75, etc.) suggest the existence of a dominant fracture set.

B. Fracture Orientation

- The study used stereographic projections and dipmeter logs to orient fractures.
- *Example*: In **Well Omn 64**, Fractures F1 and F2 were successfully oriented by combining core and dipmeter stereonets.

C. Fracture Mineralization

- Most fractures were **sealed**, often by bitumen, anhydrite, or barite, making them **barriers** to fluid flow.
- **Open fractures** (or partially mineralized) were rare but critical for fluid transport.

D. Friction Striations and Fault Indicators

- Several types of striations were observed:
  - **Subhorizontal** (indicating strike-slip motion).
  - **Subvertical** (indicating normal faulting).
  - A mixed regime also appears common, confirming the complexity of local stress fields.

E. Clay-Silt Layers and Stylolites

- Clay-silt interbeds (called “silts”) played a role in limiting vertical fracture propagation.
- **Stylolites**, mostly horizontal, were abundant and associated with vertical stress and secondary silica cementation, reducing porosity and permeability.

4.5. Key Conclusions

- The Hassi-Messaoud North reservoir is affected by a complex but **structured fracture network** dominated by one or two orthogonal sets of subvertical joints.
- **Fracture density increases near faults**, confirming the influence of deep-seated tectonics on reservoir structure.
- **Open fractures** are rare but crucial for reservoir performance; the high proportion of **sealed fractures** suggests a limited natural connectivity.
- **Core analysis remains the most reliable method** for fracture detection, while dipmeter and borehole imaging tools must be cross-validated against physical samples for accuracy

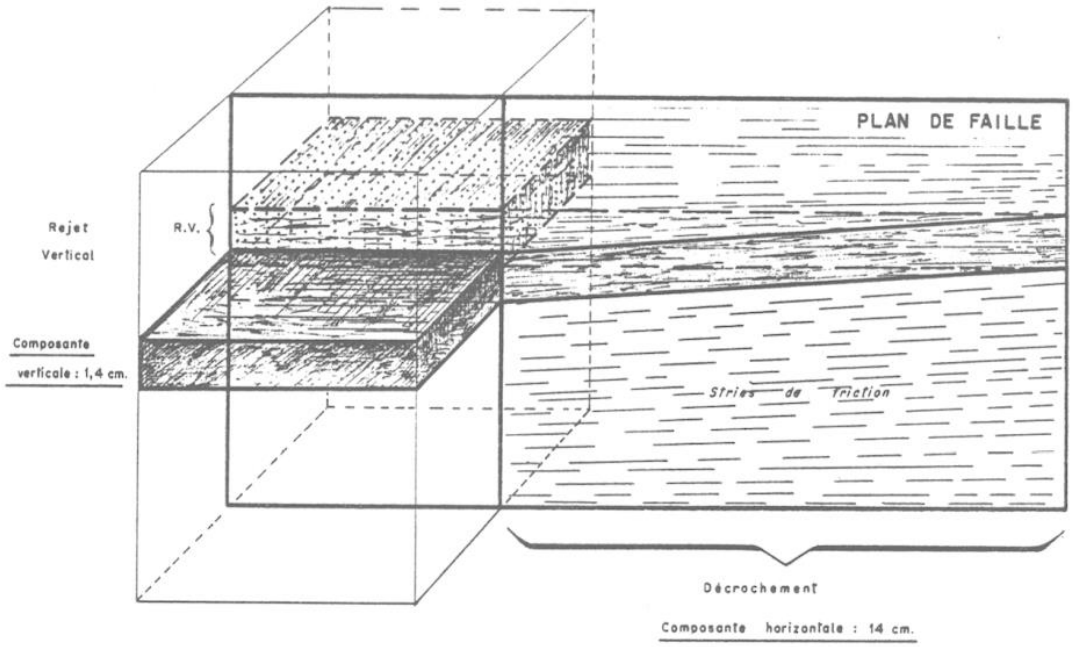

Figure 11 : Example of rejection observed on core: horizontal displacement 10 times greater than vertical displacement Omp 67; core no. 1; fragment 22

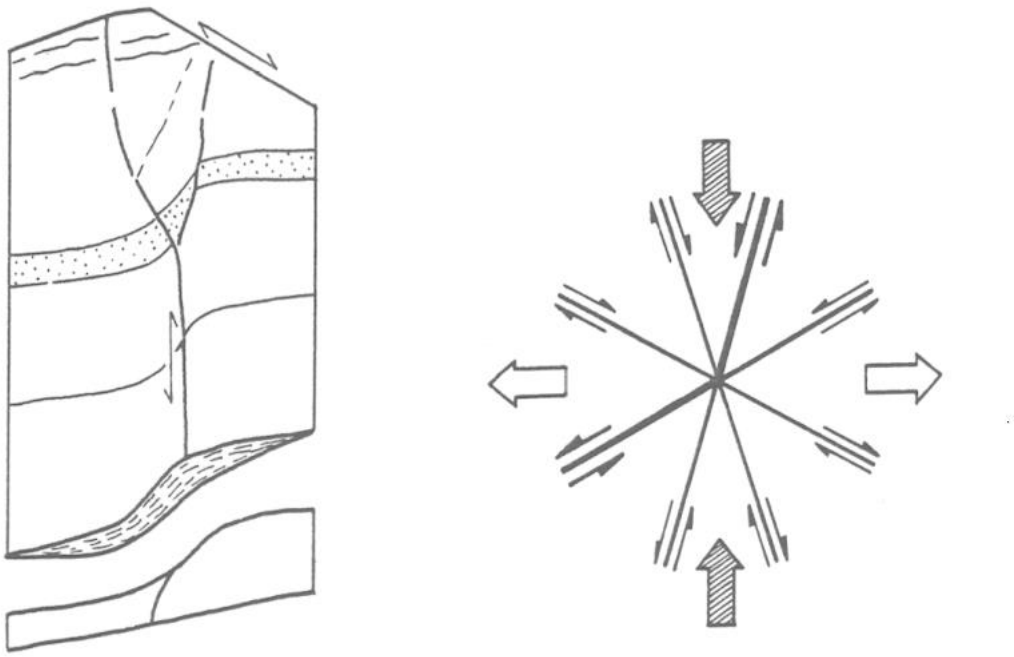

Figure 12 : Microfault associated with a double set of wedges (asymmetrical movement)

Omk: 57; elevation 3420.90 m

CHAPITER 2 :

Image tools and precissing description

Introduction

The accurate structural and geological characterization of subsurface formations is critical for optimizing hydrocarbon exploration and production. Recent advancements in borehole imaging technologies have enabled detailed visualization of the borehole wall, allowing for direct identification of fractures, bedding planes, faults, and sedimentary structures.

Among the most widely used tools are the **Ultrasonic Borehole Imager (UBI)** and its higher-resolution variant, the **Ultrasonic Borehole Micro-Imager (UBMI)**, which operate by emitting ultrasonic pulses to generate high-resolution acoustic images of the borehole wall. In contrast, the **Circumferential Borehole Imaging Log (CBIL)** utilizes ultrasonic transducers to produce continuous 360° acoustic scans, particularly effective in wells with opaque drilling fluids.

In addition, tools such as **EMAGER** (Electromagnetic Imager) and **ERTH** (Electro-Resistivity Thin-bed High-resolution imager) provide resistivity-based imaging solutions. These tools are especially useful in formations with conductive or thinly laminated lithologies, enhancing the detection of conductive fractures and micro-resistivity contrasts

1. **Classification of Borehole Imaging Tools by Operating Principle:**

1.1. Ultrasonic (Acoustic) Imaging Tools :

are visualized and interpreted. By emitting high-frequency sound waves into the borehole fluid and capturing their reflections from the borehole wall, these tools produce continuous, high-resolution images that reveal critical geological features. Unlike optical imaging, ultrasonic tools are highly effective in opaque or oil-based drilling environments, making them particularly suitable for deep, complex reservoirs. They play a key role in detecting fractures, bedding planes, and faults, and are widely used in structural geology, reservoir characterization, and wellbore stability studies.

1.1.1 Oil-Base Microlmager (OBMI) :

This solution for imaging in nonconductive muds pairs cutting-edge technology with a simple, time-honored principle of resistivity logging. While logging, the pads of the OBMI tool are applied against the borehole wall, where a thin layer of nonconductive mud is between the pad face and the formation. In accordance with the four-terminal or short-normal method of measuring resistivity, an alternating current is injected into the formation between the two electrodes at opposite ends of each pad. The unique electronics inside the OBMI pad and cartridge measure the potential difference between paired button electrodes at the center of the pad. From this value, the resistivity of the invaded zone Rxo in the small interval of the formation opposite the sensors is accurately and quantitatively calculated using Ohm's law. The schematic below shows a pad applied against the borehole wall, with possibly a small standoff.

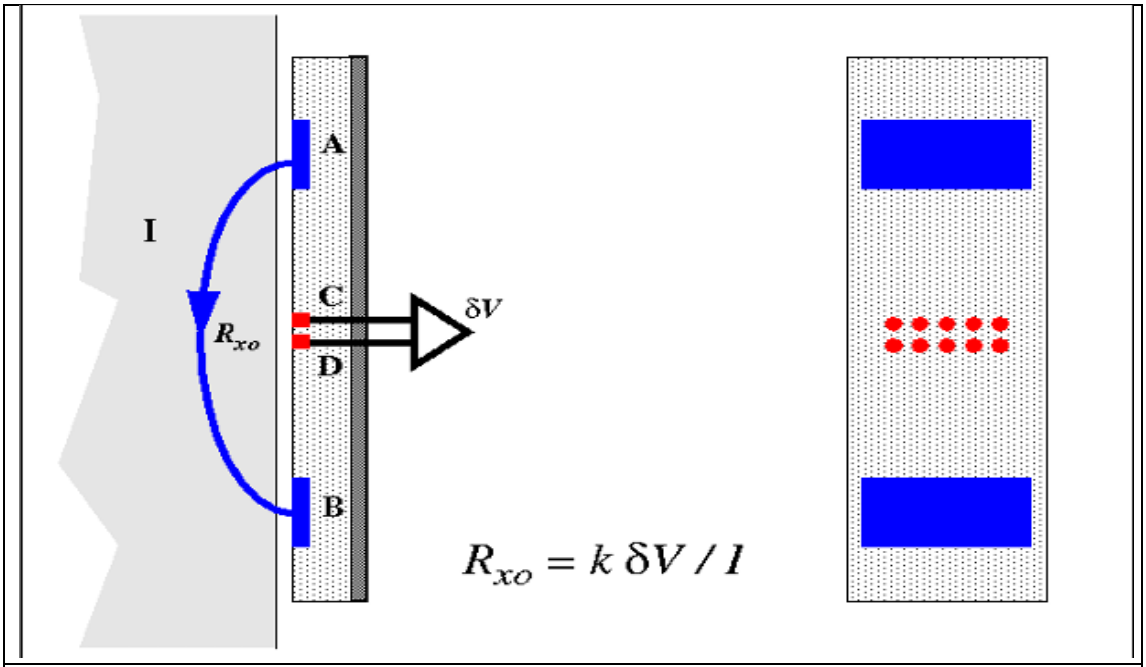

Figure 13:Schematics showing side (left) and front (right) of the OBMI pad

An AC current I is injected between the current electrodes A and B via the formation. Two button sensors measure the voltage drop &V in the formation facing the sensors. An AC current I is injected into the formation between the two current electrodes A and B, and the potential difference DV between two small voltage sensors C and D is measured. The resistivity Rxo of the small interval of formation opposite these sensors is then given by the equation:

$$R_{xo} = k\frac{\delta V}{I}$$

Where K is geometrical factor

Although it may not be obvious that this equation would apply when a layer of nonconductive mud exists between the pad and the formation, mathematical modeling and bench experiments, and indeed over 10 years of successful logging, demonstrate that the equation works well for all nonconductive muds commonly used in the oilfield and over a wide range of Rxo values, provided the mud layer is not too thick.
The OBMI tool has four pads on four arms spaced at 90 degrees around the borehole. On each pad, five pairs of sensors are placed between current. The five Rxo measurements from each pad can then be displayed as a five-pixel wide image of the formation resistivity at the borehole wall. The voltage sensors are spaced vertically and horizontally at 0.4 inch apart, giving the pixels a nominal size of 0.4 x 0.4 inch.

Figure 14: OBMI tool and OBMI image log vs. core

The tool vertical resolution is stated as 1.2 inches. This means the thinnest bed for which the width can be measured is 1.2 inches (3 nominal pixels). A bed with a width of far less than 1.2 inches may be detected, but its apparent width could be misleading Three depths of investigation have been quoted. All three values were obtained by modeling. The 3.5-inch value for "invasion" follows the conventional definition of depth of investigation, namely: the distance of an invasion front from the borehole wall for which the tool reads the average of Rxo and Rt. The 0.5-inch value quoted for a "small object" is the distance of the front face of a small cube, with sides equal to the tool resolution (here 1.2 inches) from the borehole wall for which the tool reads the average of Rxo and resistivity of the cube. The third value is the "electrical penetration" parameter used in dip determination. It allows for features apparently on the borehole surface that are recessed into the formation. This parameter depends on resistivity contrast and dip magnitude. The value quoted is an average value.

	OBMI	DUAL-OBMI
Number of pads	4	2 x 4 = 8
Pixels per pad	5	
Pixel size	0.4 x 0.4 inch	
Vertical resolution	3 x nominal pixel = 3 x 0.4 inch = 1.2 inch	
Log sampling rate	0.2 inch	
Coverage in 8 inch hole	31.8 %	Max. 2 x 31.8% = 63.6 %
Depth of investigation	Invasion: 3.5 in - Small object: 0.5 in - Dips: 0.2 in	
Resistivity range	0.2 to > 10,000 ohm-m	
Rxo Accuracy	20% for 1 – 10,000 ohm-m	
Sensitivity to stand-off	0.5 inch at 10 ohm-m, 0.25 inch at < 1 ohm-m	
Max. logging speed	3600 ft/hr	3000 ft/hr
Max. T	160°C (320°F)	
Max. P (OBMT-D, -H)	25 kpsi	
Max. P (OBMT-B, E, -F)	20 kpsi	
Hole size (OBMT-B, -D)	6.5 – 16 inch	
Hole size (OBMT-E,-F,-H)	6 – 16 inch	
Conveyance	Wireline or TLC (Tough Logging Conditions)	

Table 01 : OBMI and Dual-OBMI specifications

The Rxo value given by the OBMI tool is good to about 20% between 1 and 10,000 ohm-m. Beyond these limits, the response becomes less quantitative, but bed boundaries and other features can still be imaged. The maximum standoff that the tool can tolerate increases with the formation resistivity Rxo, and decreases with mud resistivity Rm. Because Rm varies typically by a factor of 5 between muds, Rxo is the more important factor. The table above gives two average values.

The purpose of the standard button resistivity LQC display (next figure) is to help identify artefacts in the image due to pad-liftoff (poor pad contact), signal strength too strong/weak and/or noise. LQC is an important part of interpretation since the first task of interpretation is to identify artefacts. The contents of the tracks and the checks to make are described below. As mentioned earlier, each pixel of the LQC image indicates the status of the corresponding resistivity value in the OBMI image. Please note that pad A has a green azimuth curve running down the middle

The LQC image (see below) always has pad A to D from left to right:

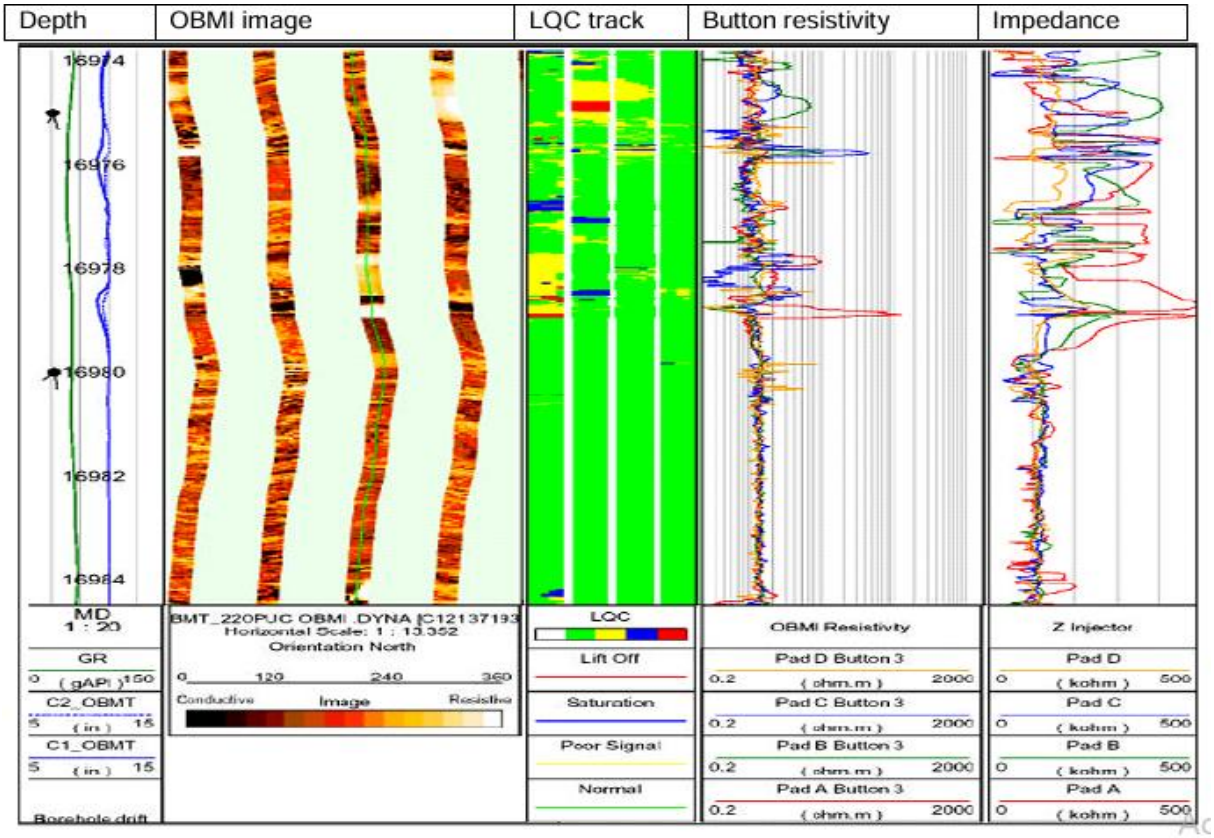

Figure 15 : OBMI LQC display
(Source : document Schlumberger).

Meaning of the flags in the standard button resistivity LQC display:

- Green on the LQC image indicates normal data. All other colors indicate an abnormality.

- **Red** usually indicates pad liftoff, when standoff becomes so important that the buttons no longer read the formation resistivity. Liftoff may be caused by rugose hole, caves, hole elongation, inability of arms to open fully in deviated or spiral holes etc... Red may also indicate that the formation resistivity exceeds 10,000 Ohmm, the tool's upper resistivity limit. If an induction log is available (just to indicate high or low resistivity, since the AIT cannot read above 2000 Ohmm), or from local knowledge, it is usually easy to know which of the two meanings of the red flag applies .

- **Blue** means the signal is too strong This is nearly always signaled for just a short time. since the gain (automatic) and applied voltage will usually adjust quickly to the signal strength. Blue is often associated with a sudden change in formation resistivity, e.g. when a fracture is encountered.

- **Yellow** covers all the other causes of poor/bad signal for which the tool cannot unambiguously attribute a cause. In casing or extremely low resistivity formations (eg. < -0.1 Ohmm), at the onset of liftoff or high resistivity, a yellow flag may be raised.

It must be emphasized that the LQC image must be used with care since the diagnostic may be ambiguous. This may happen in case of pad liftoff and high formation resistivity. In other cases. especially with yellow flags, the flag may indicate that the resistivity value measured is non quantitative but not entirely invalid. Le image features such as bed boundaries may still be valid. For example, if you see dipping beds clearly in the OBMI image and abnormal flags in the LQC image at the same time, the beds are very probably real .

The crucial factor in obtaining a good OBMI image is pad contact. Therefore firstly the calipers should be studied in the usual way. In addition, the injection impedance curves give a direct measure of pad contact. When the formation resistivity is low compared to the mud resistivity (which is usually the case since Rm-200.000 Ohmm), the injector impedance curves measure essentially the impedance of the mud layers between the injection electrodes and the formation at each of the pads. For a given mud. this means how much standoff there is. Since mud resistivity can vary by a factor of 5 for oil/water ratios between 95/5 to 70/30, the absolute values of OZx may vary greatly For 95/5 mud, the injector impedance can measure up to 250.000 Ohm when pad contact is minimal. For 70/30 mud, it can be as low as 50.000 Ohm More to the point, if the curve is very active, it means the hole is rugose and there may be pad liftoff problems .

When formation resistivity is very high (>10000 Ohmm) the injector impedance curves will sense both the mud and formation impedances in series since the formation impedance is no longer negligible

1.1.2 Ultrasonic Borehole Imager (UBI) :

The UBI tool is an acoustic borehole televiewer based on ultrasonic imaging technology. This technology is uninfluenced by mud type, although there are limitations to the solid particles content and thus to mud weight (see Measurement and mechanical specifications for UBI). One transducer is placed into a rotating sub, which rotates at 7.5 revolutions per second. The tool electronics generates a firing rate depending on the desired sampling. The ultrasonic transducer rotates about 2 inch from the borehole wall and repeatedly sends a short ultrasonic pulse towards the borehole. After traveling through the mud, the main part of this pulse is reflected back to the transducer. The transit time and amplitude of the echo are measured. Knowing the acoustic velocity in the borehole fluid, the transit time is converted to radius and images of borehole geometry are produced.

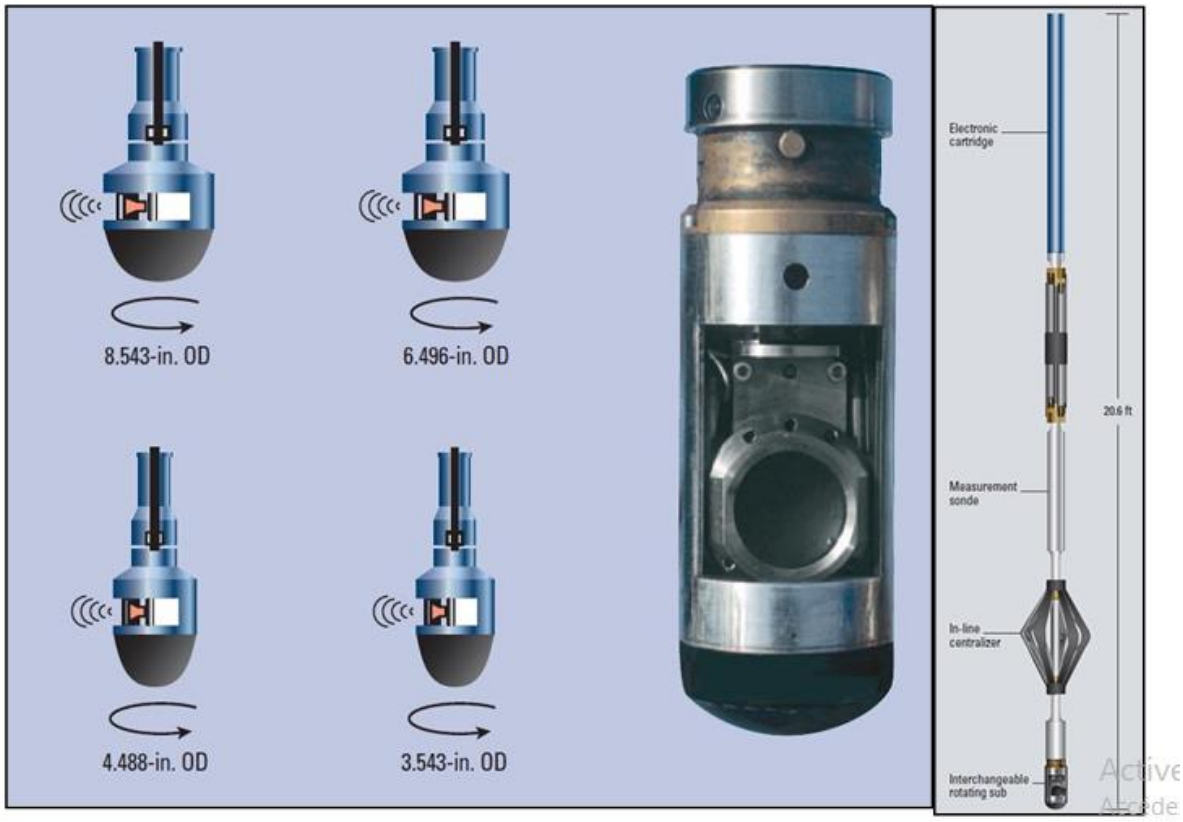

Figure 16 : Different sizes of rotating transducers (to provide optimum standoff)
(Source: Schlumberger)

The transit time is a quantitative measurement, but in fractures and breakouts the echo can be too small to be reliably detected. The echo amplitude depends on the angle of incidence of the ultrasonic beam on

The borehole, on the rugosity of the borehole, on the hardness of the borehole and on the propagation distance. Fractures, breakouts and soft formations give low amplitude echoes.

Through advanced borehole imaging and stress analysis applications, borehole stability and breakout information can be derived from the accurate borehole cross section as measured by the UBI tool. For openhole measurements and for casing internal geometry measurements in
which casing resonance is not needed the UBI tool's transducer results in high-resolution images.

Key applications of the UBI tool are:

- fracture identification and analysis
- structural dip analysis
- borehole stability evaluation
- hole shape analysis
- rock textural analysis

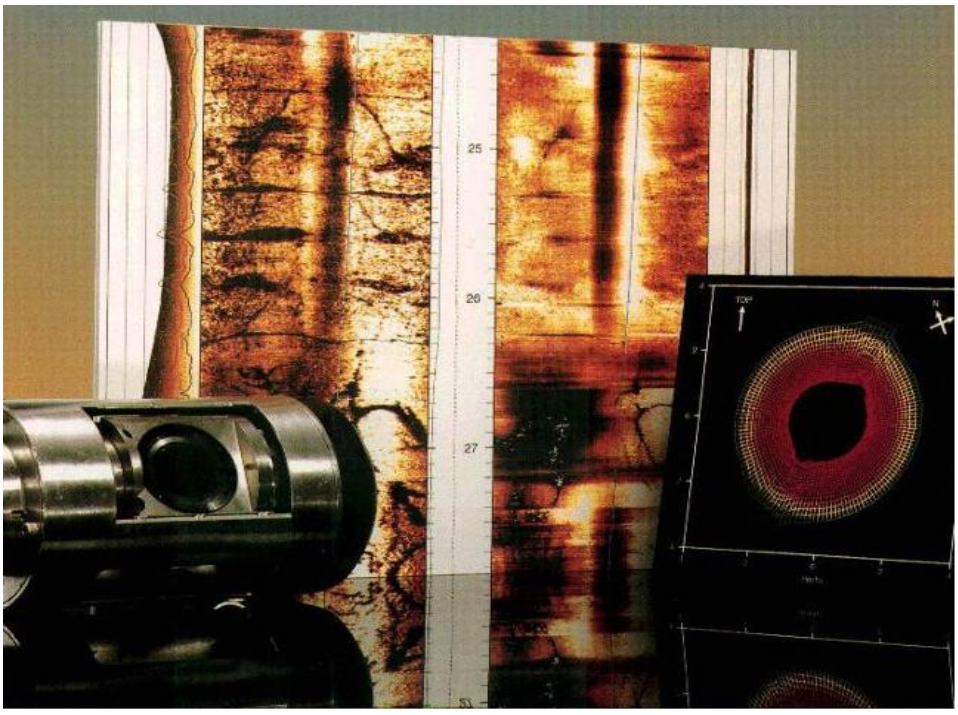

Figure 17 : Processed UBI image log with amplitude image (L), transit time image and cross-section (R)(*Source: "document Schlumberger")*

The transducer is both a transmitter and a receiver, transmitting an ultrasonic pulse and receiving the reflected pulse. The transducer is focused to improve resolution, to reduce eccentering effects and to improve echo detectability in out-of-shape holes and on rough surfaces. It can be operated at two frequencies, 250 kHz and 500 kHz, according to the selected working mode. Selecting the most suitable transducer subassembly to reduce attenuation in heavy fluids and to maintain a high signal-to-noise ratio optimizes the distance traveled by the ultrasonic sound pulse in the borehole fluid. The low-frequency mode has a better penetration through heavier muds, while the high-frequency mode provides finer resolution, but it is restricted to light muds and boreholes in good condition.

	UBI tool
Output	Borehole images, amplitude and transit time
Logging speed	425 to 2125 ft/hr (130 to 648 m/hr) depending on desired resolution
Borehole size	4 7/8 to 12 7/8 inch
Vertical resolution	0.2 inch at 500 kHz (max. logging speed 425 ft/hr) 0.4 inch at 250 kHz kHz (max. logging speed 850 ft/hr) 0.6 inch at 250 kHz kHz (max. logging speed 1275 ft/hr) 1.0 inch at 250 kHz kHz (max. logging speed 2125 ft/hr) Azimuthal sampling 2.0 inch or 2.6 inch
Accuracy	Borehole radius +/- 0.12 inch (absolute) Resolution: 0.003 inch at 500 kHz
Depth of investigation	Borehole wall measurements
Mud type / weight limitations	WBM < 15.9 lbm/galUS (1.91 g/cm3) OBM < 11.6 lbm/galUS (1.39 g/cm3)
Combinability	Bottom-only tool, combinable with most tools
Temperature rating	350°F (177°C)
Outer diameter (OD) w/o sub	3 3/8 inch
Length	21 ft
Weight	377.6 lbm (171 kg) with 7-inch USRS-B sub
Tension	40,000 lbf (177,930 N)
Compression	11,000 lbf (48,930 N)

Table 02 : Measurement and mechanical specifications for UBI

1.1.3. CBIL (Circumferential Borehole Image Log) ;

The Baker Atlas CBIL (Circumferential Borehole Image Log) is an acoustic borehole imaging device, which produces an image of the borehole wall by continuously recording the amplitude and travel time of an ultrasonic acoustic signal, reflected off the borehole wall. The result is an image, covering the entire circumference of the borehole, with 250 samples per depth increment. Vertical sample rates are 30 or 60 samples/foot. The amplitude of the reflected signal is sensitive to variations in acoustic impedance as well as the surface roughness of the formation, both of which depend largely on lithology. The amplitude image is therefore used for identification and orientation of geological features. The travel time reflects the diameter of the borehole and can be used as a high-resolution caliper or to further characterise structural features.

During acquisition, the image data are oriented either to magnetic north, using a built-in magnetometer, or to a pre-defined tool body mark. When logging horizontal sections, the tool body mark option is always used, whereas for vertical and deviated sections, either option may be used. The advantage of the magnetometer mode is that images are automatically oriented to magnetic north during recording. If the tool body mode option is used, the raw data require further processing in order to correctly

orient the images. During acquisition, irregular logging speed or tool sticking events may result in artificial “squeezing” or “stretching” of the data along the borehole axis. This effect is corrected for during processing by analysing the high resolution accelerometer data recorded simultaneously.

The image cylinders are “cut” and unrolled to produce standard rectangular displays. In this report, the industry-standard brown-white colour scheme is used for display of amplitude images. Low amplitude areas are imaged as brown, and high amplitude (hard) areas in paler shades. If travel time displays are used, short travel time (low borehole radius) is imaged as light and long travel time (high borehole radius) as dark grey. This way, areas of enlarged borehole, such as washouts, breakout or open fractures are imaged in dark colours on both types of images. Planar features (e. g. bedding planes, faults, and fractures) intersecting the borehole at an angle other than 0° or 90° appears as sinusoids in the images.

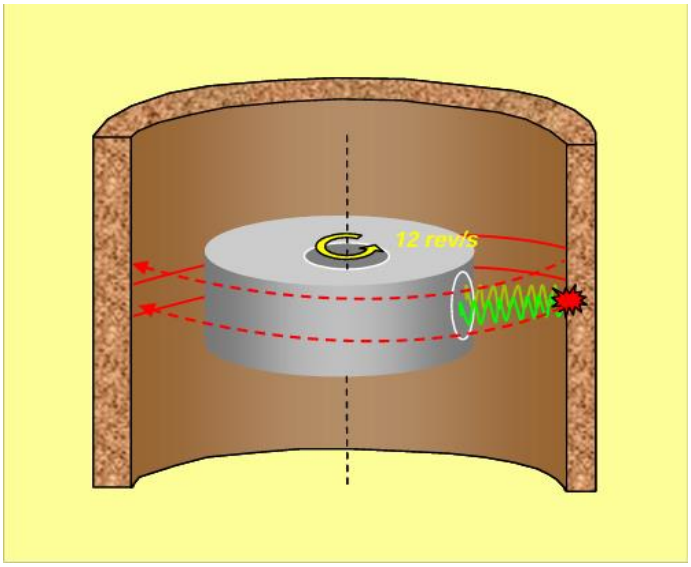

Figure 22 : The rotating transducer measures amplitude and travel time of an ultrasonic signal, reflected off the borehole wall. The resulting data helix contains 250 samples/revolution and 30,40 or 60 vertical samples/ft

1.2. Electrical and Electromagnetic Imaging Tools :

Electrical and electromagnetic borehole imaging tools provide crucial insights into formation properties by measuring variations in electrical resistivity across the borehole wall. These tools are especially effective in conductive or finely laminated formations where acoustic imaging may be limited. By using pad-mounted electrodes or induction-based sensors, they generate detailed resistivity images that help identify conductive fractures, thin beds, and lithological boundaries. Their high vertical resolution and sensitivity to fluid content make them indispensable for reservoir characterization, fracture mapping, and petrophysical analysis in complex geological environments.

1.2.1 EARTH Imager

The Baker Atlas EARTH Imager is a resistivity imaging device specially designed for logging in non conductive (oils base) mud. It is a six-arm tool with each arm carrying an electrically conductive pad which transmits current into the formation through 8 button electrodes (Figure 3). During logging the pad is kept at a constant voltage, so that the amount of current transmitted to the formation through each electrode depends directly on the resistivity of the formation, in a manner similar to a micro-laterolog tool. This enables acquisition of high-resolution resistivity image data from the area immediately adjacent to the borehole wall. The vertical sample rate is typically 60 or 120 samples/ft. The pad width is approximately 2.45 inches, which results in a 78% circumferential coverage of a 6 inch borehole or 56% of an 8.5 inch hole. The resistivity imager may be connected with the CBIL tool and the two sets of images can be acquired simultaneously or during individual runs, e. g. to reduce stick-and-pull caused by the resistivity tool arms.

The image is oriented by recording the position of a tool body mark (aligned with pad 1) to magnetic north (tool azimuth) and the high side of the borehole (relative bearing). During post acquisition processing the image is reoriented with the “edges” of the image corresponding to either geographic north or borehole high side. Accelerometer correction is carried out as for the CBIL data (see above) to correct for stick-and pull effects.

The images are displayed using the brown-to-white colour scheme (also used for the CBIL), with dark brown colours for low resistivity and white for high resistivity. It is important to note that since the log is acquired in a resistive mud environment, cavities and open fractures will appear bright (resistive) on the image opposite to what is seen on the CBIL and on conventional water-based mud (STAR) resistivity images.

Figure 23 : EARTH Imager tool

2. OBMI & UBI Data acquisition :

2.1 Signal processing :

The data were processed in our data services centre on the Schlumberger GeoFrame platform. Computed dip results and images were produced using standard processing parameters. The main objective was to provide a continuous log of formation structure in the form of interpreted dip results, fracture analysis and near wellbore images. For the UBI, Amplitude and Transit Time variations of the ultrasonic signal, recorded by the tool are converted into Amplitude and Radius color images after speed correction, depth alignment, electrode equalisation and static normalisation using a histogram equalisation technique. Further contrast enhancement was achieved by using a sliding 2 m normalisation window to produce the dynamic images.

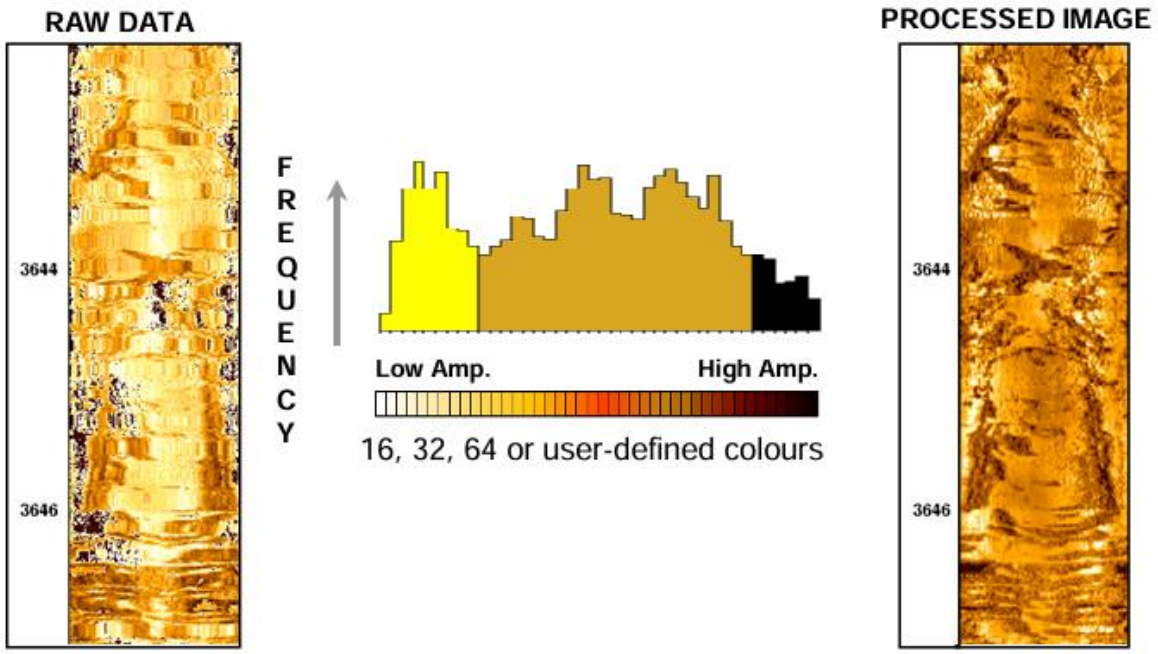

Fugure 18 : RAW DATA and PROCESSED IMAGE

The OBMI and UBI data are processed and analysed to generate resistivity and amplitude/transit-time images of the near borehole wall structures using the following GeoFrame workflow :

- **Data Load** : Loading of DLIS acquisition data into GeoFrame project
- **GPIT Survey:** Checking the inclinometry data
- **BorEID :** Primary corrections to image data (button equalization, speed correction..)
- **BorNor :** Static and dynamic normalisation of image data
- **BorView :** Interactive graphic tool for image interpretation
- **StatPack :** Statistical analysis of dip results and generation of dip azimuth vector plots
- **SediView :** Determination of the structural dip based upon a local curvature axis technique

2.2 General Purpose Inclinometer Tool (GPIT) checks :

Dip computation and speed correction requires inclinometry data provided by the GPIT tool. These data were checked using the GPIT_Survey module of GeoFrame. The corresponding plots for the Main and Repeat logs

2.3 Speed correction :

Where the Wireline cable depth at surface and data acquisition depth down-hole differ then it is essential to make a correction. The method used for the OBMI data is accelerometer-based

and estimates the speed and the depth of the tool by using simultaneously the cable depth and the integration of the z-axis accelerometer data. A Kalman filter method is used to find the best estimates of speed and depth that are consistent with both measurements.

2.4 Image Generation :

BorNor is the GeoFrame module that performs image enhancement prior to graphical display. It uses an histogram equalization method to optimise the use of a given number of colours in a given interval based on a histogram distribution of the resistivity values. Two types of normalization are performed:

- **Static Normalization :**

is a single computation where the colour classes are based on a measurement distribution histogram defined over the whole logged interval. Changes in colour represent gross variation in the measurement and correspond to major changes in porosity / cementation. Static normalized images are used to determine large scale structural and stratigraphic breaks.

- **Dynamic Normalization :**

is the result of multiple computations, repeated at regularly spaced positions over user specified depth interval using a window of relatively short interval (0.6 m in this well). Changes in colour represent small-scale features, corresponding to small changes in porosity, texture and mineralogy. Dynamic normalisation enhances the image texture and the sedimentary structures. The main application of dynamically enhanced images is manual dip picking and image facies analysis.

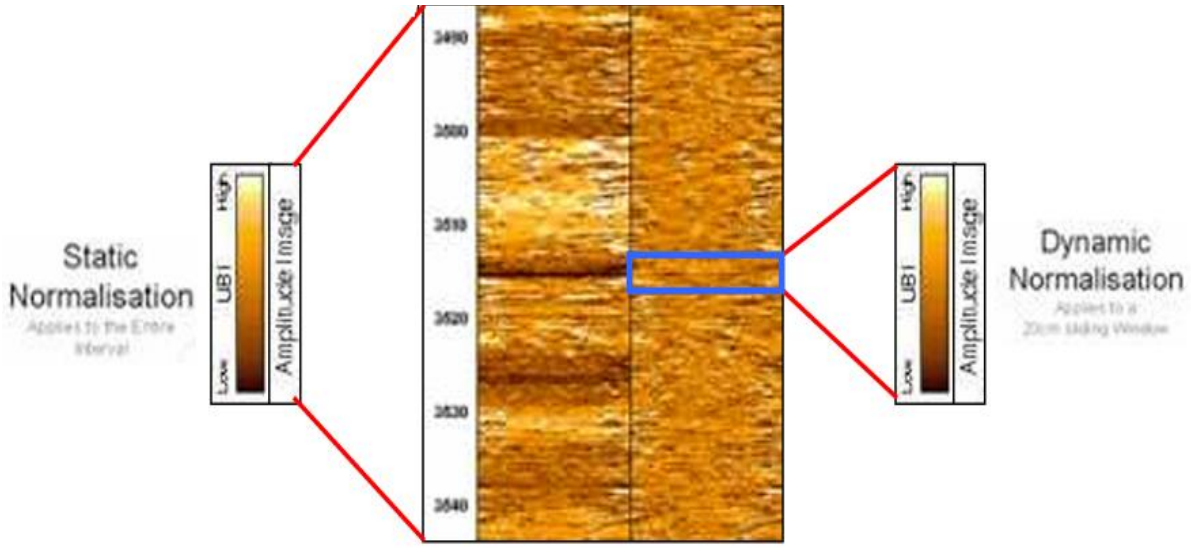

Figure 19: Image Normalization. Example from UBI image.

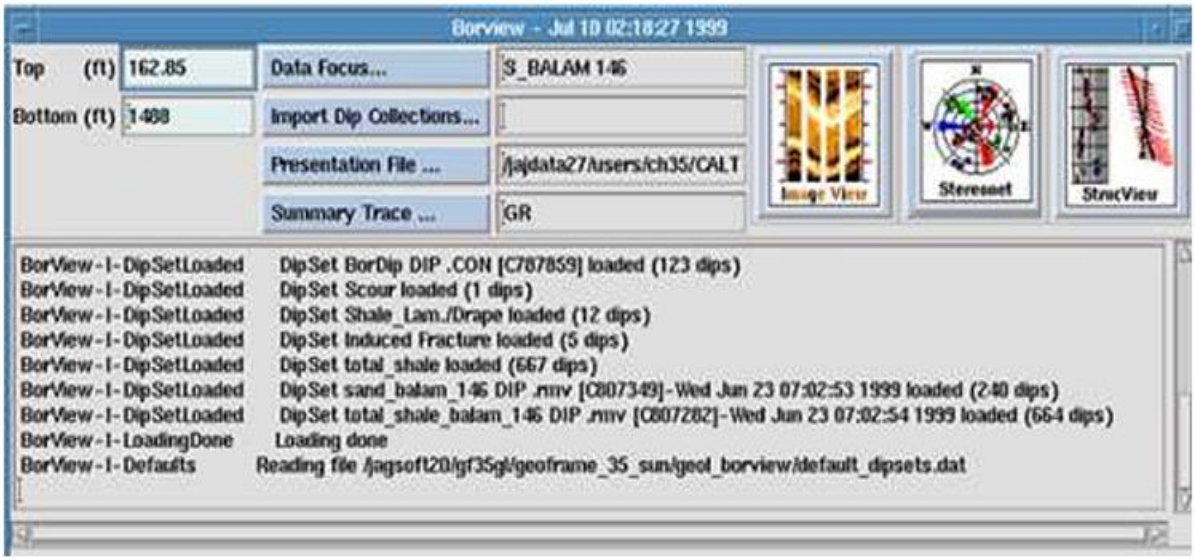

Figure 20 : BorView : Interactive graphic tool for image interpretation.

Three modules are available: the **ImageView** image analysis and dip picking, the **Stereonet** module for dip trend analysis and the **StrucView** module for module for structural cross-section modelling.

StrucView allows the interpreter to draw structural cross-section models based on structural dip data:

- a geological type of structure (normal fault, reverse fault, fold etc) is chosen to guide the analysis of the data. This choice is based on the structural appearance of the dip set (dip drag) and the available geological knowledge of the field.

- the axis of the cross section is computed and a geological cross section is generated using a technique based on similar fold construction from dip data developed by Arnaud Etchecopar: StrucView, Etchecopar, A., Bonnetain, J.L., 1992 – Cross-sections from Dipmeter data. AAPG bull, V. 76, No.5, P(621-637). StrucView: a method to model structures from dips in the vicinity of wells.

- **StatPack :** Statistical analysis of dip results and generation of dip azimuth vector plots
- **SediView :** Determination of the structural dip based upon a local curvature axis technique developed by Arnaud Etchecopar: SediView, Etchecopar, A., Dubas, M.O., 1992 - Automatic method for geological interpretation of dips. Proceeding of the SPWLA meeting. (Oklahoma City).

- the original dip set is filtered based on quality and coherence between successive dips

- a local curvature axis is computed- the structural dip is identified with a quality factor

- the structural dip component is removed from the original dip set so sedimentary dip analysis can be performed.

2.5 Structural dip analysis :

SediView is a module of GeoFrame that is used to determine and to remove structural dip. SediView is based on the analysis of the local curvature axis of sedimentary structures and structural deformations.

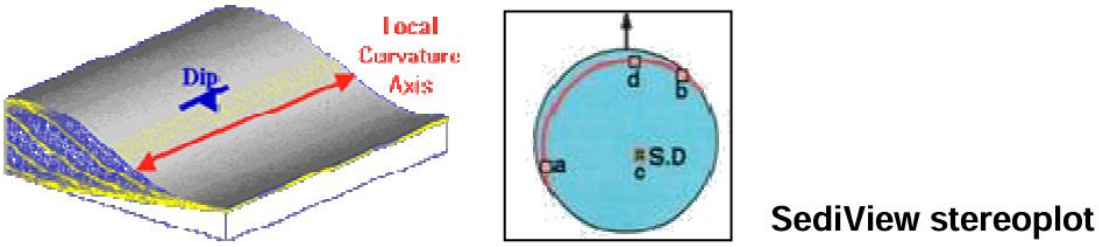

Figure 21 : SediView stereoplot

The bed boundaries that were picked on the borehole image (all dips but the fractures and the faults) are analysed by SediView with the following steps:

- Filtering by quality and continuity of dip data
- Determination of the structural dip and its uncertainty
- Structural dip removal

SediView provides a fast & accurate method for structural dip determination, even in clean sand intervals where structural dip (SD) cannot be estimated with the traditional approach (SD picked only in shale intervals). This module also enables the identification of low angle structural events such as unconformities and of the sedimentary dip component.

3. Comparative Table of Borehole Imaging Tools

Tool	Operating Principle	Image Type	Optimal Environment	Main Application
UBI	Ultrasonic pulse (rotating)	Acoustic image	Opaque mud, deviated wells	Fracture and bedding interpretation
UBMI	High-resolution ultrasonic pulse	High-resolution image	Hard, micro-fractured formations	Microfracture detection, fine textural analysis
CBIL	360° ultrasonic scanning	Circumferential image	Muddy or oil-based drilling fluids	Full-wall structural mapping
ERTH	Pad-based resistivity imaging	Resistivity image	Thinly laminated or conductive zones	Thin-bed resolution, conductive fracture mapping
EMAGER	Electromagnetic resistivity	Resistivity image	Conductive formations or saline muds	Detection of conductive fractures, clay

Table 03 : Comparative Table of Borehole Imaging Tools

4. Identifiable Parameters from UBI, UBMI, CBIL, ERTH, and EMAGER :

4.1. UBI, UBMI, CBIL *(Ultrasonic Acoustic Imaging Tools):*

- **Open and sealed fractures :**

Detection of natural fractures, analysis of aperture and filling material.

- **Fracture dip and azimuth :**

  Measurement of orientation and inclination of structural features.

- **Fault planes :**

  Identification of slickensided or offset fault surfaces.

- **Bedding planes and lamination :**

  Visualization of sedimentary layers and discontinuities.

- **Friction striations :**

  Observation of striated surfaces indicating tectonic movement.

- **Surface roughness and textural details:**

  Differentiation between sealed and open fractures.

.

- **Vertical heterogeneity**

  Detection of lithological variations and structural discontinuities.

4.2. ERTH and EMAGER *(Electrical / Electromagnetic Resistivity Imaging Tools):*

- Formation resistivity.
- Conductive fractures.
- beds and laminations.
- Lithological boundaries.
- Shale-rich zones / clay seams.
- Microfractures (in some cases).

CHAPITER 3 :

Results and Discussion

Introduction

Our study is based on the analysis of acoustic and electrical imaging obtained from the Earth Imager, CBIL (Circumferential Borehole Imaging Log), and UBI-UBMI tools, provided respectively by Baker Hughes and SLB. In most wells within the study area, both imaging techniques were combined to achieve a more comprehensive interpretation. However, in certain specific cases, only one of the two methods (either acoustic or electrical) was used.

Acoustic imaging is primarily used for interpreting fractures, faults, and breakouts, while electrical imaging is employed to analyze bedding dips, stratification, and to distinguish between resistive and conductive fractures.

In this study, we utilized subsurface geological and structural data obtained from the following drilled petroleum HMD wells: OMF-502, OMG-832, ONI-353, OMG-513, and OMG-812.

In conclusion, the combination of acoustic and electrical imaging proves to be the most effective approach for obtaining both qualitative and quantitative interpretations of fracturing, faults, bedding, dips, and breakouts.

1. Geological interpretation of EARTH Imager & CBIL data :

Help Standard list of diptypes used for EARTH Imager/CBIL interpretation in the Hassi Messaoud Field.

Dip Category	Description	Dip Tadpole Colour	
SILT BEDDING	Internal bedding in intra reservoir mudstone ("silt").	Green	
SILT TOP	Bounding top surface in intra reservoir mudstone ("silt").	Purple	
SILT BASE	Bounding bottom surface in intra reservoir mudstone ("silt").	Orange	
SST BEDDING	Internal bedding in sandy lithology. Used mainly for beds thought to be originally low angle, but also for inclined beds, which are not believed to be cross-bedding.	Yellow	
CROSS BEDDING	Closely spaced laminae dipping at a high angle relative to, and often cut by, low angle sandstone beds. In quartzite these occur mainly in clean sand intervals.	Magenta	
LOW AMP FRAC	Narrow high angle feature showing a strong low amplitude (dark) contrast on the CBIL. Likely to represent an open or partially open fracture. Wide open fractures show resistive contrast on the EARTH Imager but narrower ones may show as conductive (also see section 4.1).	Red	
HIGH AMP FRAC	Narrow high angle feature showing a strong high amplitude (bright) contrast on the CBIL. Likely to represent a closed fracture.	Pink	
RFRAC	Resistive fracture. Fracture seen as resistive (bright) on the EARTH Imager but without associated low amplitude contrast on the EARTH Imager. May represent a silica-cemented fracture ("vein").	Scarlet	
RFRAC DIS	As above, but covering only a fraction of the borehole circumference.	Violet	
CFRAC	Conductive fracture. Fracture seen as conductive (dark) on the EARTH Imager with high amplitude (bright) or no contrast on the CBIL. Likely to represent a closed fracture, clay-lined or cemented by conductive minerals such as pyrite.	Blue	
MFRAC	Mixed fracture. Used for mixed conductive/resistive fractures on EARTH Imager (rare) probably representing closed mixed fill fractures.	Brown	
BREAKOUT	Parallel patches of enlarged borehole, occurring at opposite sides of the borehole and parallel to the borehole axis. Interpreted as drilling-induced compressive failure (borehole breakout).	Olive	

Table 04 : Standard list of diptypes used for EARTH Imager/CBIL interpretation in the Hassi Messaoud Field

1.1.results of WELL OMF-502 Image log:

EARTH resistivity data and CBIL from the 6inch section of the near vertical well OMF 502 of the Hassi Messaoud Field, Algeria.

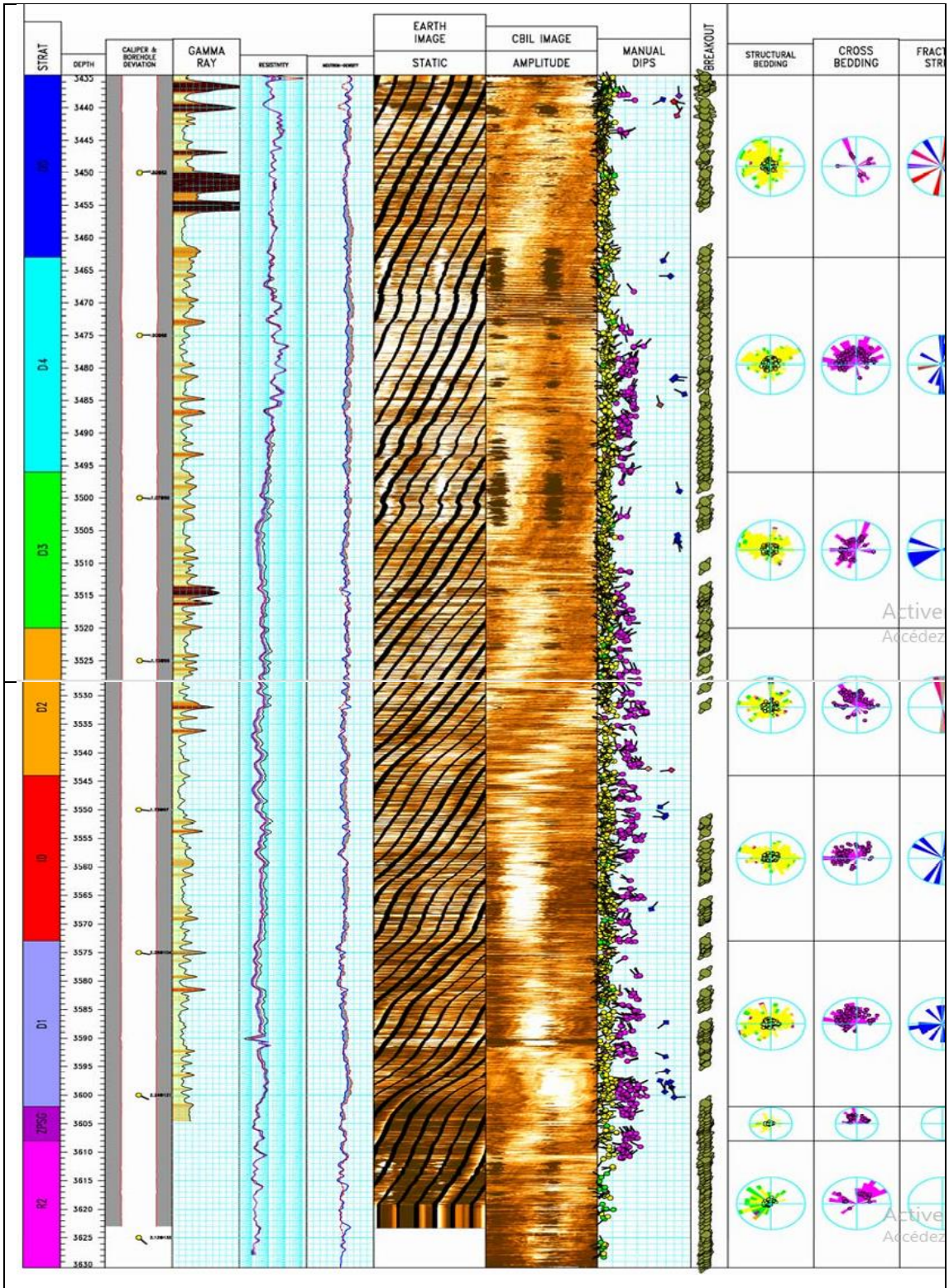

Figure 24: Compressed scale plot summarising the main results of the Image log interpretation.

1.1.2. WELL OMF-502 Image log interpretation :

The following are the main conclusions drawn from this study. A compressed scale summary plot, displaying the main data

- EARTH Imager and CBIL data is of very good quality. Bedding and fractures are well resolved, and high confidence structural and depositional analysis is possible. Fracture characterization is based on both resistivity and acoustic image information and the distinction between open and cemented fractures is quite certain.
- Structural dip is dominantly towards the NW. The following structural dip zonation has been defined:
    - 3435-3446m: 02°/261° (NE)
    - 3446-3476m: 03°/325° (NW)
    - 3476-3494m: 02°/028° (NE)
    - 3494-3559m: 02°/310° (NW)
    - 3559-3577m: 01°/038° (NE)
    - 3577-3630m: 03°/286° (NW)

- Large-scale high angle cross-bedding is common below 3474m. Above this depth cross-bedding is practically absent, which is thought to reflect an increasing intensity of bioturbation towards the top of the D4 and throughout the D5 unit. Cross-bed azimuths show a NW dip trend, commonly observed in the field.

- The fracture density is very low through out the studied interval. As usual most fractures show a conductive contrast on the EARTH Imager log along with low amplitude in CBIL, suggesting that they are filled or partially filled with clay, pyrite or other electrically conductive minerals. Sparse resistive fractures probably represent relatively wide open fractures. Fracture orientations define four clusters with a mean dip value of 67°/160° (NE-SW strike), 59°/271° (N-S strike), 60°/012° (E-W strike) and 70°/094° (N-S strike) respectively. No faults have been identified.

- Borehole breakout is present throughout the logged section. The location of breakout on the borehole wall is roughly NE–SW throughout the imaged interval, with only very minor variations, indicating that the maximum horizontal stress is oriented NW–SE.

1.2.results of WELL OMG-832 Image log:

EARTH resistivity and CBIL acoustic borehole image data from the 6 inch section of the vertical well OMG-832 of the Hassi Messaoud Field, Algeria.

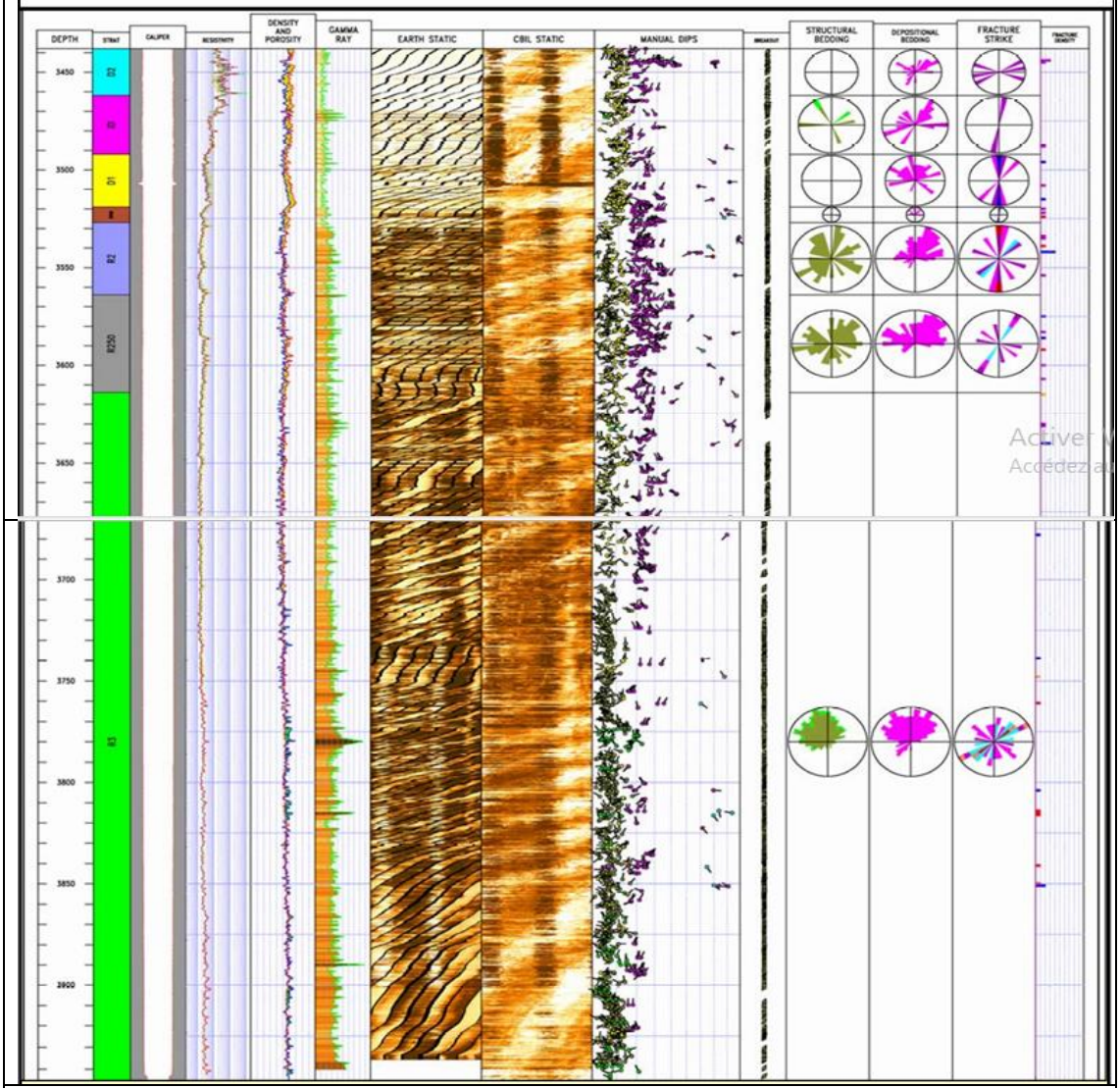

Figure 25 : Compressed scale plot summarising the main results of the Image log interpretation.

- Compressed scale plot summarising the main results of the image log interpretation. Depositional bedding (cross bedding) on rose histograms has been rotated to remove structural dip. For the entire interval, probable siltstone bedding (olive) has been discriminated from shale bedding (green) based upon GR value . the following figures are oriented to North.

1.2.1 WELL Image OMG-832 log interpretation :

The following are the main conclusions drawn from this study. A compressed scale summary plot, summarising the main results is shown in Figure 25.

- Both EARTH Imager and CBIL image quality is generally very good. Structural and depositional analysis was of high confidence due to fairly large dataset. Fracture characterization is of high confidence and is based both on EARTH Imager and CBIL observations.
- Overall structural dip is low, with a mean azimuth trending towards the NW (5°/334°). The interval represents a single structural zone.
- Common cross-bedding in the sandstones shows a broad range of dip azimuths, but with a mean dip/azimuth of 12°/003°. Four distinct dip clusters are observed with minor fluctuations in between. Over the entire interval the palaeocurrent direction fluctuated from NNE at the lower part to NW above it then at the upper part again to NNE with a transitional phase in between where the palaeocurrent direction was to the N.
- Fractures are sparsely populated throughout the logged interval, but noticeably more abundant above 3650m. Both potentially open and closed fractures are observed, of which the former are more common. Two distinct fracture trends are identified with the open fractures. The main direction, striking NE–SW, has a mean dip/azimuth of 68°/137°. Subordinate directions with a mean dip/azimuth of 69°/099°. The closed fractures show a broad range of fracture plane azimuths.
- Borehole breakout occurs throughout the logged interval. Breakout orientation is roughly NE–SW, with the maximum horizontal stress inferred to be in the direction 122 – 302°.

Depth	Structural Dip	Mean Dip (Dip/Azim)	Comments
3438 – 3946m	Shale and siltstone bedding	5°/334° (n=864)	High confidence low dip towards NW.

Table 05: Structural dip zonation in well OMG-832.

Zone	Depth Range (m MD)	Mean Dip (Dip/Azim)	Comments
D	3438 – 3619.5m	12°/014° (n=534)	High confidence. Overall dip angle greater than 10° with azimuth trends to the NNE with minor fluctuations.
C	3619.5 – 3656m	16°/359° (n=76)	High confidence. Overall dip angle higher than 10° with an azimuth trend to the N with minor fluctuations.
B	3656 – 3724m	16°/329° (n=130)	High confidence. Overall dip angle greater than 10° with azimuth trends to the NW with minor fluctuations.
A	3724 – 3946m	9°/012° (n=128)	High confidence. Overall dip angle close to 10° with azimuth trends to the NNE with minor fluctuations.

Table 06 : Depositional dip

1.3. results of WELL ONI-353 Image log:

EARTH resistivity and CBIL acoustic borehole image data from the 6 inch section of the vertical well **ONI-353** of the Hassi Messaoud Field, Algeria

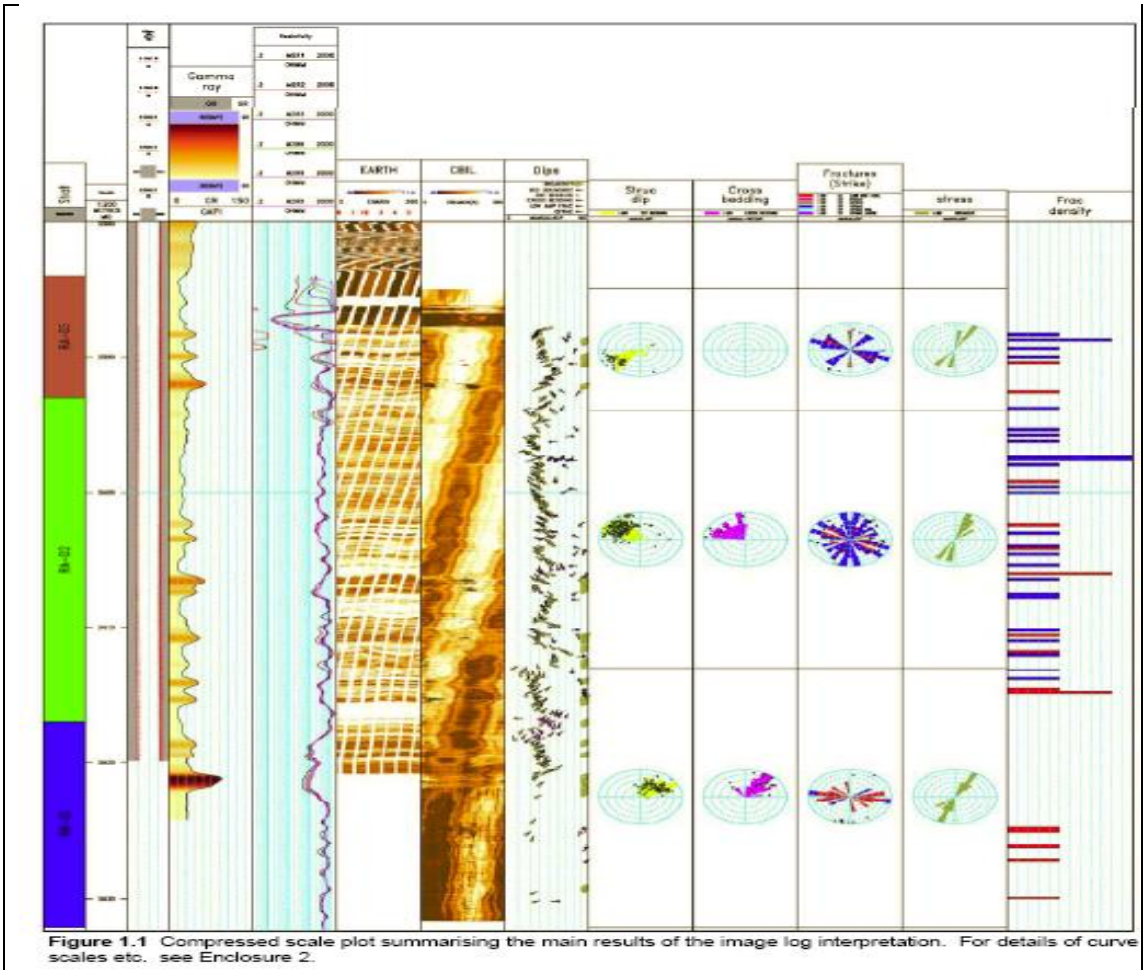

Figure 1.1 Compressed scale plot summarising the main results of the image log interpretation. For details of curve scales etc. see Enclosure 2.

Figure 26 : Compressed scale plot summarising the main results of the image log

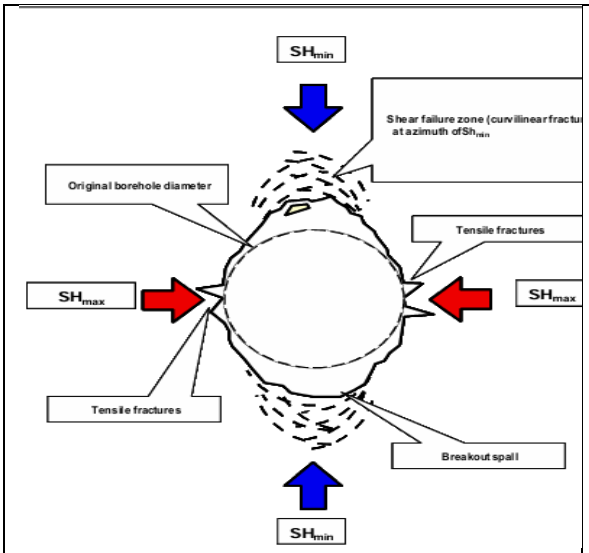

Figure 04 : Tensile fractures Tensile fractures Tensile fractures Tensile fractures Simplified figure of a transverse cross-section through a borehole, illustrating the different drilling induced failures that may occur. In a vertical well the orientation of breakouts and tensile fractures indicate the orientation of the in situ stress field. The orientation of breakout marks the direction of the minimum horizontal stress, whereas the location of drilling induced tensile fractures marks the direction of maximum horizontal stress.

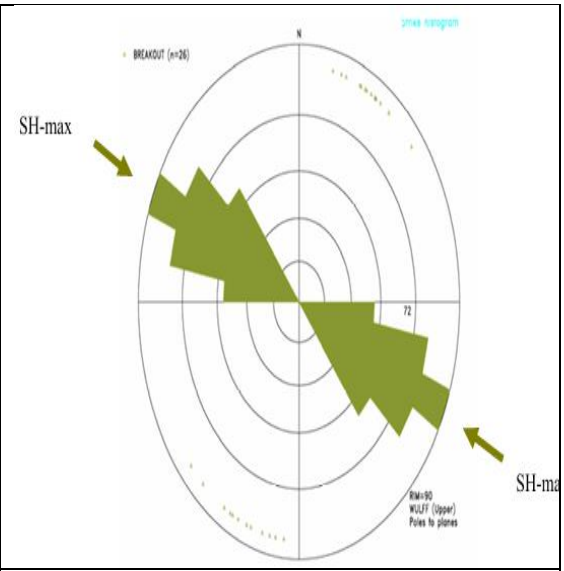

Figure 05 : Breakout through the logged section indicating that the maximum stress is oriented WNW-ESE.

Formation	Mean dip, structural zones	Depth	Comments
Zone3	33°/232°	3394-3385m	Dominantly good image quality. Very high angle dip & sandstone bedding relatively very well resolved.
Zone2	30°/309°	3413-3394	
Zone1	24°/46°	3432-3413m	

Table 07 : Structural Dip Zonation. The listed values are mean dips of bedding classified as SST BEDDING & BED BOUNDARY. The values calculated above represents the structural dip for each zonation.

Age	Formation/Unit	Depth (m MD)
Cambrian	Hercynian Uncorformity	3384
	RA-D3	3384
	RA-D2	3393
	RA-ID	3417
	RA-D1	3447(EXTRAPOLÉ)
	RA-TD	3434.5

Table 08 : Stratigraphic breakdown of the logged section, provided by Sonatrach. The top of the Cambrian is at 3384m (Hercynian Unconformity). The top of the image logs is at the base of the 7inch casing at 3387.2m (log depth).TD is 3434.5m and the bottom of the image data is at 3432m.

1.3.1 WELL Image ONI-353 log interpretation :

The following are the main conclusions of the study:

- The EARTH and CBIL images are of good quality in the whole section. Bedding are well resolved on the EARTH Imager. Fractures and breakouts are clearly seen on both CBIL and EARTH Imager.
- Structural dip analysis is based on sandstone bedding, yielding a high confidence structural dip. Throughout the studied interval three structural zones have been identified: zone1, zone2 and zone3 with highly dip bedding in the whole interval.
- Structural dip rotates from NE to NW and changes to the SW, across the logged interval.
    - 3432m to 3413m 25°/045° (NE)
    - 3413m to 3399m 30°/310° (NW)
    - 3394m to 3385m 33°/231° (SW).
- Paleocurrent analysis was based on cross-bedding dips. The whole section is dominated by high angle structural dip as indicated above, hence cross-bedding are difficult to identify. They are more frequent in the upper part of the ID unit and some intervals in D2 unit indicating a high energy deposition environment. They show an unimodal orientation between NE and NW.
- Fractures are seen as discontinuous dark lines on the CBIL, and many are uncertain as they may represent borehole wall artefacts or other steep formation features especially in this well, indicating that open and partially open fractures are rare. Examples of such fractures can be seen e.g. at 3414.5 3415m. They are not considered likely to contribute significantly to production.

- The majority of fractures are of the “CFRAC” type; they appear as conductive on the EARTH Imager with no contrast on the CBIL, indicating that they are filled with an electrically conductive substance. The most fractured intervals are 3388.4-3390.3, 3394, 3395.3-3396.3, 3397.4-3398.2, 3407.5-3408.3, and 3411-3413.5m. It is noteworthy that most of those fractures are related to the structural event with an evident high angle dip in the whole section and three structural zones. However, most of the closed fractures in the present well are probably cemented with clay or pyrite, and many of them are seen with a visible off-set on the resistivity image, indicating a bedding displacement.
- In the present well borehole breakout occurs sporadically throughout the studied interval. The orientation is constant NNE-SSW, indicating a WNW-ESE orientation of the maximum horizontal stress. An average azimuth of 25° is obtained for the whole section.

2. OBMI - UBI Geological Interpretation :

Help Standard list of diptypes used for EARTH Imager/CBIL interpretation in the Hassi Messaoud Field.

Glossary	
UBI	Ultrasonic Borehole Imager.
GPIT	General Purpose Inclinometry Tool.
DEVI, HAZI	Borehole deviation angle & azimuth (deg).
P1AZ	Pad 1 Azimuth (deg).
C1-C2	Caliper axis 1-3 and 2-4 respectively.
GR	Gamma Ray.
AZ	Accelerometer Z component.
CS	Cable Speed.
TENS	Cable Tension.
Static	Fixed window image normalization (total interval).
Dynamic	Sliding window image normalization (0.6 m interval).
AO10 to 90	AIT one foot resolution resistivity at 10 to 90 inches depth of investigation.
TNPH	Standard resolution Neutron Porosity.
RHOB	Standard resolution formation bulk density.
σH , σh	Present day *in-situ* maximum & minimum horizontal stresses respectively.

Table 09 : Standard list of diptypes used for OBMI – UBI

2.1.results Ultrasonic Borehole Imager – UBI OMG-513 :

Ultrasonic Borehole Imager – UBI data from the 6 inch section of the vertical well **OMG-513** of the Hassi Messaoud Field, Algeria

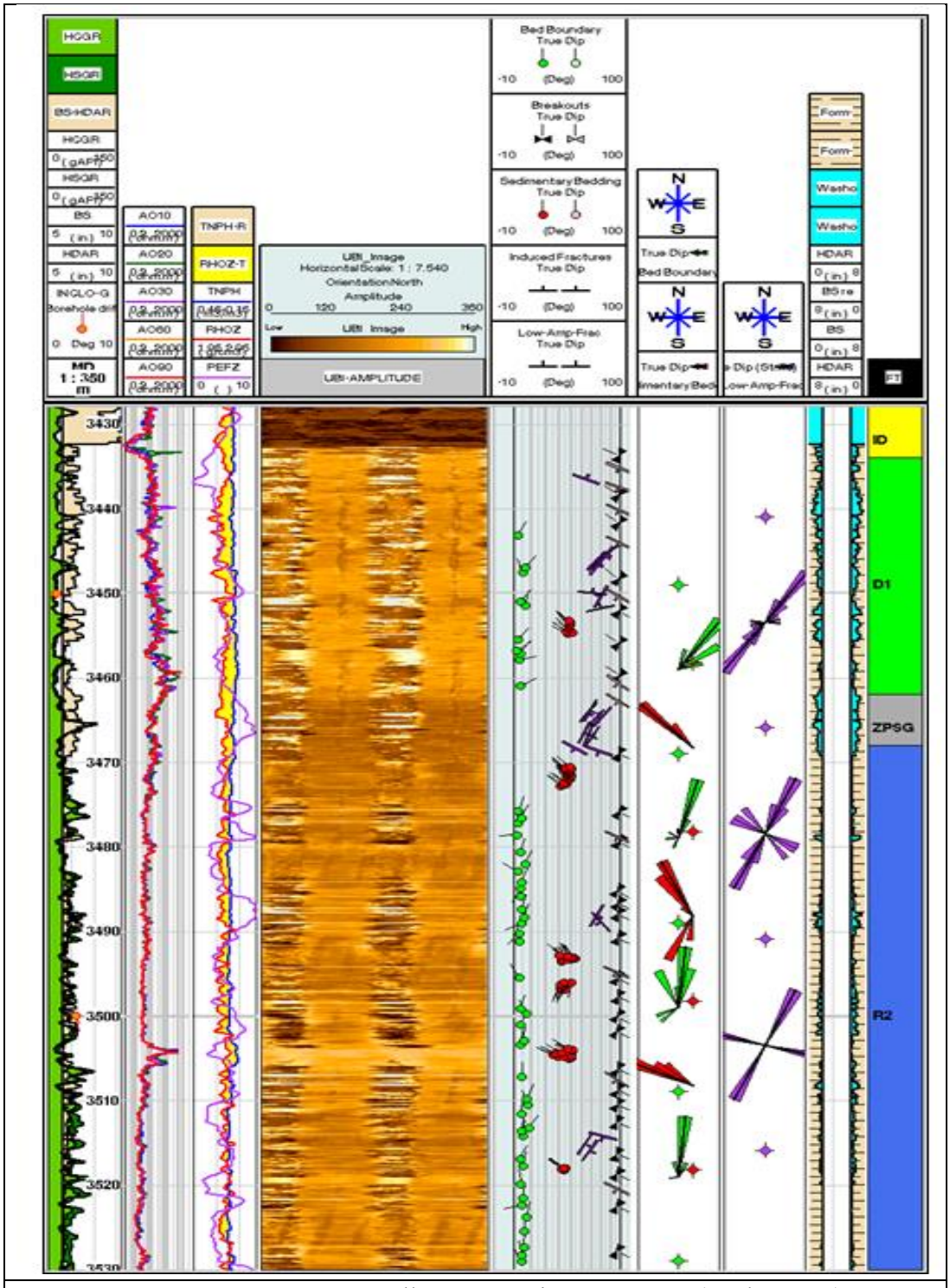

Figure 27 : OMG-513 Well Interpretation Summary (Scale 1:350)

Geological Object	Number of dips	Mean Orientation (Dip &Azimuth)
Bed Boundary	48	3.9 / 6.1
Sedimentary Bedding	63	34.4 / 311
Induced Fractures	11	88.5 / 211.1
Low Acoustic Amplitude Fractures	23	67.4 / 129.5
Breakout	26	88.7 / 122.7
Total	171 interpreted dips	

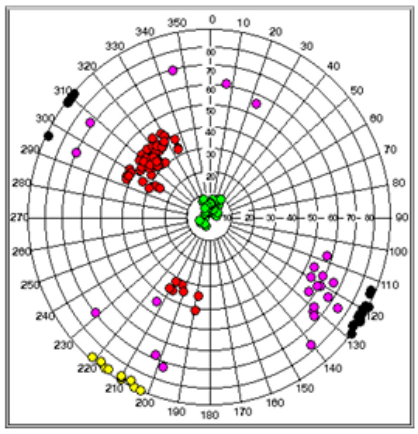

Table 10 : Dip Classification & Statistics

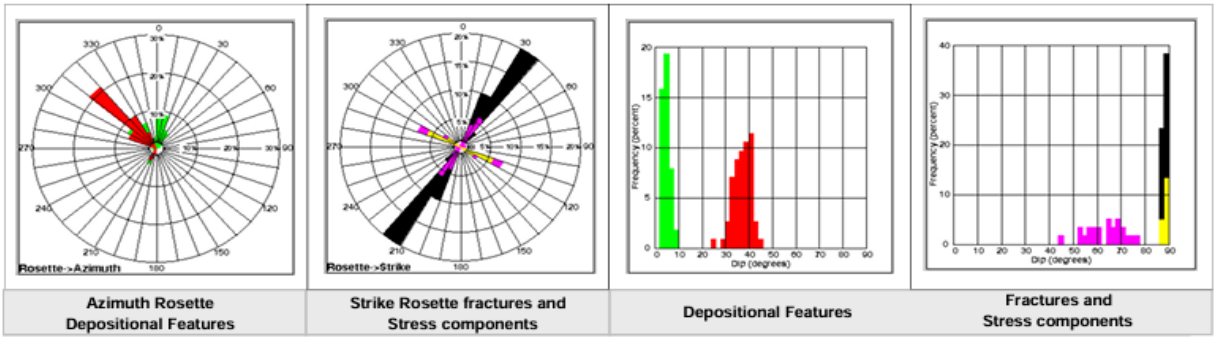

Figure 28: Dip Statistics from UBI Image Analysis.

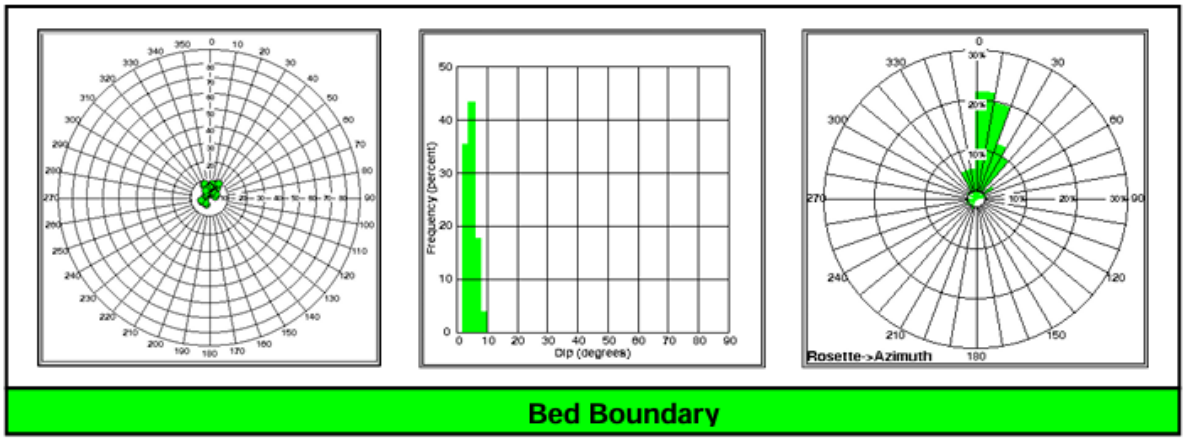

Figure 29 : Bed Boundary Statistics

2.1.1. Ultrasonic Borehole Imager – UBI OMG-513 Interpretation :

The following are the main conclusions of the study:

- The quality of the UBI dataset acquired along the studied interval of OMG-513 well enabled extracting a medium confidence dips that were used for the structural and sedimentary interpretation.

- The UBI image quality in well OMG-513 was severely affected by extensive deep and wide breakouts in places, which affected the geological analysis in the most affected intervals. The overall quality was however rated Moderate (C).

- A total number of 171 manual dips was identified on the UBI image over the logged interval, which provided average statistical data for the structural and the sedimentological analysis.

- A low number of bed boundaries was identified due to hole conditions but also to the acoustic artifacts caused by the UBI signals. As the result, the confidence of the magnitude structural dip to NNE was rated Low. We recommend to use the UBI - OBMI combination as OBMI images allow picking low magnitude structural dips with much more accuracy than UBI images due to its principle of measurement.
- The analysis of the paleo-current directions identified on the sedimentary beds show a main trend to NW and a minor trend to SW.

- 23 low acoustic amplitude fractures with a dominant NE-SW strike and a minor NW-SE minor strike were identified across the logged interval.

2.2. Results UBI / UBMI Well OMG-812 :

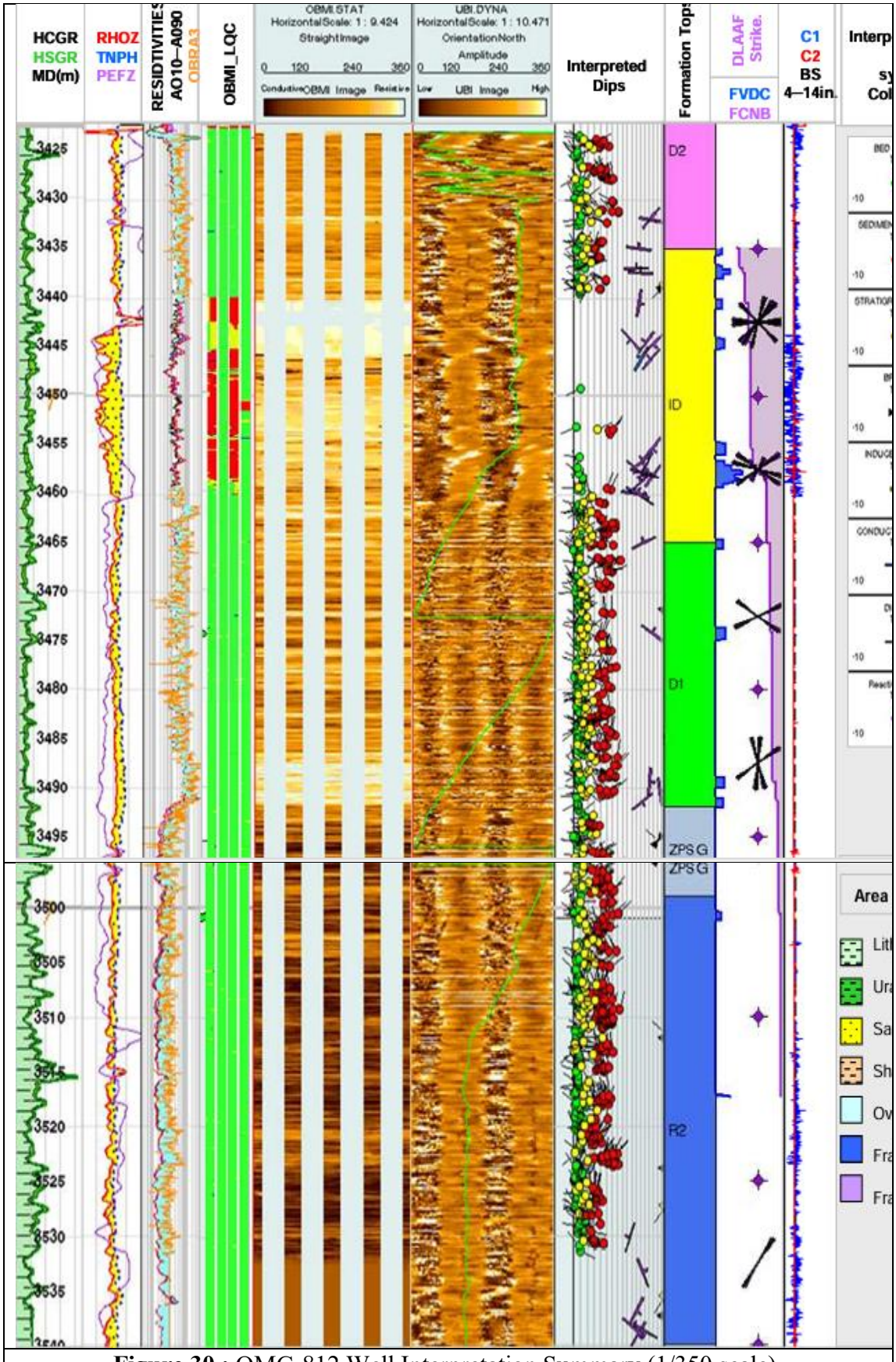

Figure 30 : OMG-812 Well Interpretation Summary (1/350 scale).

2.2.1. Fracture Morphology :

A low number of (33) fractures were observed; including two types of fractures within the Cambrian drains intercepted by OMG-812 vertical well on both UBI and OBMI images:

- Low acoustic amplitude fractures on the UBI images
- Conductive fractures on the OBMI images.

➢ **UBI Fractures :**

Discontinuous Low Acoustic Amplitude Fractures :

There were about 31 discontinuous low acoustic amplitude fractures interpreted on the UBI images with a NE-SW dominant strike and E-W and WNW-ESE minor strike trends (Figure 7). The fracture dip magnitude ranges between 50 and 94 degrees.

These fractures appear as partial dark sinusoids on the image (discontinuous trace) since they absorb more acoustic energy than the surrounding matrix. When the filling material is the drilling mud, these fractures are open, but fractures filled with clay materials can also have the same signature based on the clay/formation acoustic impedance contrast. It is therefore recommended, when possible, to calibrate the fracture analyzed from the UBI image with the fractures that observed in the core data. Centered radius image (derived from the acquisition transit time) can help in identifying possible open fractures. When the fracture is visible on both amplitude and centered radius images, it possibly corresponds to an open fracture.

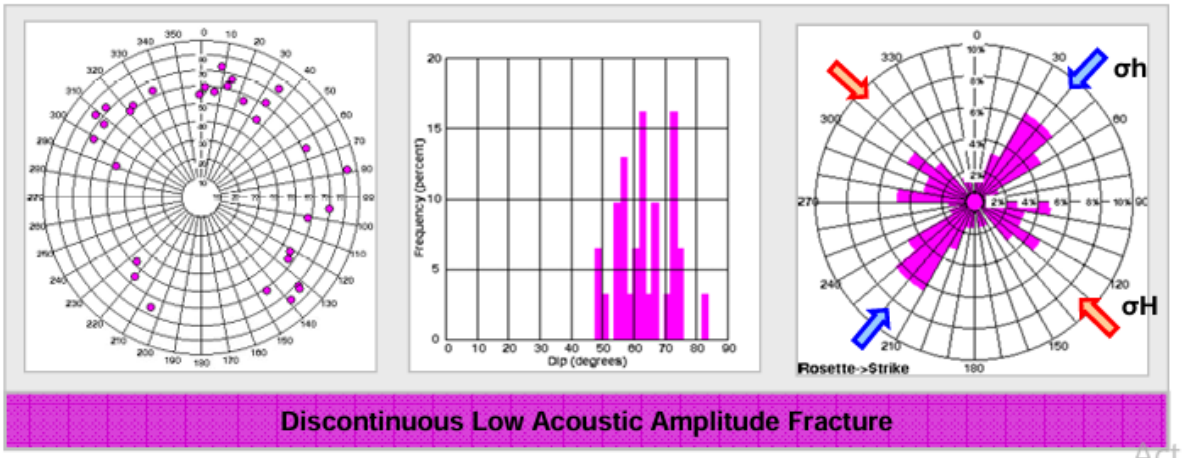

Figure 31 : Discontinuous Low Acoustic Amplitude Fracture

- **OBMI Fractures :**

Conductive Fractures :

Only two low angle conductive fractures were identified on the OBMI resistivity images characterized by a dark trace with a NE-SW and E-W strike trends within the ID.

These fractures appear as dark sinusoids on the OBMI image since they absorb more electrical current than the surrounding matrix. Conductive fractures are either filled by conductive materials such us mud, clay or pyrite.

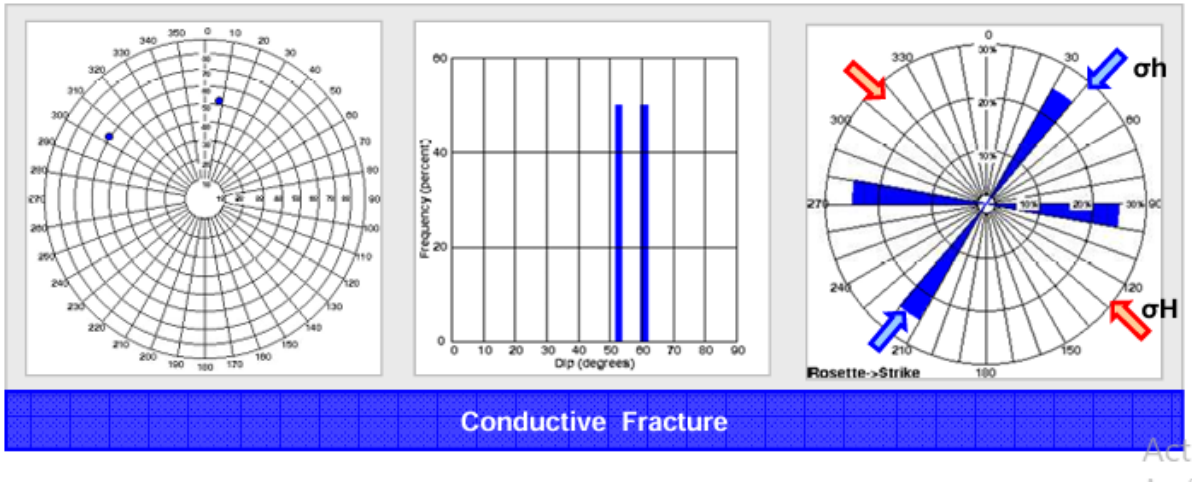

Figure 32 : Conductive Fracture

- **Fracture Distribution & Orientation :**

A wide spread of fracture distribution and orientation over the 117m Cambrian section of OMG-812 well was observed and its summarized in the following table.

Most of the fractures were interpreted within the R2 and the D1 drains with a predominant NE-SW strike trend and WNW and E-W minor strike trends.

Formation	Discontinuous Low Acoustic Amplitude Fractures	Major / Minor	Conductive Fractures
D2	2	**NE-SW** / E-W	-
ID	18	**NE-SW** / NW-SE, WNW-ESE	2
D1	5	**NE-SW** / N-S, NW-SE	-
ZPSG	-	-	-
R2	6	**NE-SW** / NW-SE, WNW-ESE	-

Table 11 : Fracture Statistics & Orientation

2.2.2. Hole Shape Analysis :

A comprehensive analysis of the borehole shape was made from UBI transit time data. The high resolution borehole radius measurement (1 azimuthal sample every 2 degrees) is calculated from transit time data after calibration with the velocity of the acoustic signal in the drilling fluid. Hence, wellbore cross-sections were generated over some zones to provide a representative indication of the borehole wall shape. Few examples are shown in the figure below.

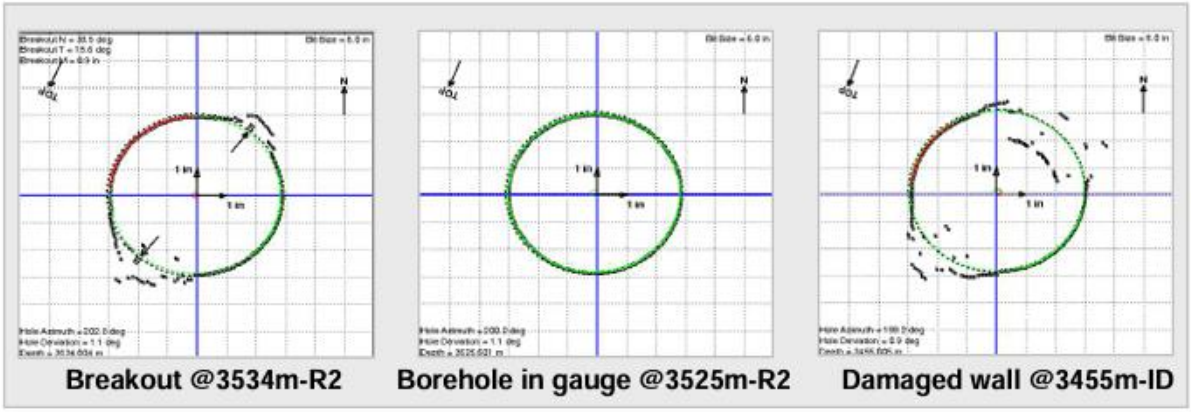

Figure 33 : Examples of Hole Shape Analysis Cross Sections

- R2: Borehole breakout is mainly developed over the drain. Only few sections are in gauge showing more stable formation especially in the upper part of the R2 (3499 to 3503m, 3515.3-3515.8m…).

Induced fractures were also identified in the bottom section of the R2 where it developed perpendicular to the borehole breakout direction.

-ZPSG: Developed borehole breakout ends at the top interval (~3492.2m).

-D1: This section of the well is less affected by the breakouts, especially the interval between 3486 and 3465m corresponding to a clean sand lithology with a low GR, (mainly < 35 GAPI), high resistivity profile and N-D cross-over.

-ID: Drain is also characterized by the development of drilling induced fractures and continuous breakouts.

-D2: Continuous borehole breakout was observed along the D2 showing up as two dark traces developed at 180 degrees apart from each other.

* As the well is vertical, the breakout orientation (NE-SW) corresponds to the present day minimum in-situ horizontal stress, which means that the direction of the maximum in-situ horizontal stress, also provided by the induced fractures, is oriented NW-SE.

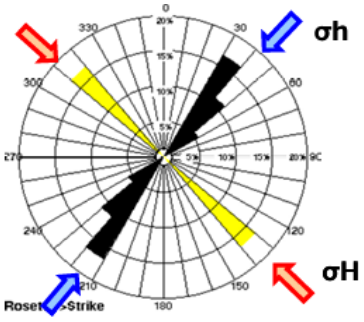

Figure 34 : Stress Components Orientation
InducedFractures (yellow) & Borehole Breakout (Black)

General conclusion

General conclusion

The integration of acoustic and electrical borehole imaging tools—namely UBI, UBMI, CBIL, and Earth Imager—has proven highly effective in the structural characterization of the Hassi Messaoud North (HMD Nord) reservoir. Each tool offers distinct advantages that, when combined, provide a comprehensive interpretation of subsurface features.

- **Acoustic imaging tools** (UBI, UBMI, and CBIL) are particularly useful for identifying and analyzing fractures, borehole breakouts, and wellbore geometry. They enable the detection of open versus closed fractures and assist in understanding borehole stability through breakout analysis.
- **Electrical imaging tools** (Earth Imager and OBMI) excel in revealing bedding planes, dip measurements, stratification, and distinguishing between resistive and conductive fractures. These capabilities are crucial for precise structural and sedimentological interpretation.
- The **Earth Imager and CBIL** combination allows for high-resolution identification of bedding dips, faults, fractures, and paleocurrent directions. These tools have enabled high-confidence interpretations in multiple wells (e.g., OMF-502, OMG-832, ONI-353).
- The **UBI and OBMI** datasets, particularly in wells like OMG-812 and OMG-513, provided additional insight into fracture morphology, stress orientation, and borehole shape analysis, despite challenges from borehole breakouts and acoustic artifacts.

Overall, the synergy of acoustic and electrical imaging methods ensures a reliable qualitative and quantitative understanding of the structural architecture of the reservoir. This integrated approach enhances reservoir modeling and supports better decision-making in field development and production plannin

References

The reviewer

Excerpt from the 2002 Communications Proceedings

Source: Schlumberger–Sonatrach WEC 2007

Source: SONATRACH 2004 – Geology of Hassi Messaoud

Document Schlumberger-Sonatrach WEC 2007

Source: Schlumberger – Sonatrach WEC 2007 document

Benayad et al.,2013, AArabian Journal of Geosciences

Excerpt from the 2002 Communications Proceedings

Source: SONATRACH 2004 – Geology of Hassi Messaoud

Source: "SONATRACH" – Geology of Hassi Messaoud, 2004

S. Mekmouche, "Description of the Hassi Messaoud Reservoir", Forum Stimulation SH/DOWELL, Hassi Messaoud, 1994

Designed by Hassi Messaoud, published by C. Sallé and J. Debyser, Technip 1976

Documents « SONATRACH 2004» : Géologie de Hassi-Messaoud

Structure and fracturing of the Hassi Messaoud field, M. Ruhland, J. Thouvenin, 1971

Source: Sonatrach / Production Division – Internal Report, 2002

Beicip/Franlab, 1979

Source: "SONATRACH" – Geology of Hassi Messaoud, 2004

After Boudjema (1987) and Beicip (1975). Modified by K. BOUSLAH

Lévêque, 1969

just to indicate high or low resistivity, since the AIT cannot read above 2000 Ohmm

J.-M. GAUTIER et al.

Allaud L. A. et Ringot J. (1969). — The high resolution dipmeter tool. The Log Analyst, (maijuin 1969).

Balducchi A. et Pommier G. (1970). — Cambrian oil field of Hassi-Messaoud, Algeria. Am. Assoc. Petrol. Geol. Memoir 14, p. 477-488.

Byramjee R. (1961). — Observations sur les brèches rencontrées dans les grès de Messaoud. Rapport GFP.A. R.G. 213 G.O.

Campbell R. I. (1968). — Stratigraphie applications of dipmeter data in mid-continent. Am. Assoc. Petrol. Geol. Bull., 9, p. 1700-1719.

The reviewer

Claret R. (1970). — Fundamentals of dipmeter interpretation. Schlumberger, New York.

Combaz A. (1967). — Un microbios du Trémadocien dans un sondage d'Hassi-Messaoud. Actes Soc. Linn. Bordeaux, 104, B, 29, p. 1-26.

Fondeur C. (1964). — Etude pétrographique détaillée d'un grès à structure en feuillets. Rev. Inst. Franç. Pétrole, 19, p. 901-920.

Friedman M. (1969). — Structural analysis of fractures in cores from Saticoy Field, California. Am. Assoc. Petrol. Geol. Bull., 53, p. 367-389.

Gartner J. E. (1966). — Application de la pendagemétrie. Rev. Assoc. Franç. Techn. Pétrole, 180, p. 59-65.

Gautier J. M. (1971). — Fracturation du champ d'Hassi-Messaoud Nord (Algérie). Etude de tecto¬ nique analytique. Thèse de 3ft cycle, Univ. Louis Pasteur, Strasbourg, 63 p.

Gilreath J. A., Healy J. S. et Yelverton J. N. (1969). — Depositional environments defined by dipmeter interpretation. Trans. Gulfcoast Assoc. geol. Soc., 19, p. 101-111.

Heald M. T. (1955). — Stylolites in sandstones. J. Geol., 63, p. 101-114.

Henry J. (1969). — Quelques exemples d'interprétation de pendagemétrie continue. Soc. of Prof. Well Log. Analysts (avril 1969).

Janot P. (1971). — Determination of the elementary matrix block in a fissured reservoir. Appli¬ cation on the Eschau field Alsace, France. Amer. Inst. min. engin., 36-38.

Gautier, J.-M., Gruneisen, P., Massa, D., & Ruhland, M. (1973). *Fracturation et analyse tectonique sur carottes de sondage. Étude méthodologique appliquée au champ d'Hassi-Messaoud Nord*. Sciences Géologiques. Bulletin, 26(2–3), 115–159. https://doi.org/10.3406/sgeol.1973.1429